

Nonlinear electron synchrotron cooling and synchrotron self-Compton flaring of TeV blazars

Dissertation zur Erlangung des Grades eines
Doktors der Naturwissenschaften in der
Fakultät für Physik und Astronomie
der Ruhr-Universität Bochum

vorgelegt von
Christian Röken
aus Gelsenkirchen



Bochum, November 2008

1.Gutachter: Prof. Dr. Reinhard Schlickeiser

2.Gutachter: PD Dr. Horst Fichtner

Datum der Disputation: 27.01.2009

Einige Teile der vorliegenden Arbeit sind bereits in Form von Artikeln mit den Titeln

Röken, C., Schlickeiser, R., "Synchrotron self-Compton flaring of TeV blazars II. Nonlinear electron cooling", A&A (2008)

Röken, C., Schlickeiser, R., "Synchrotron self-Compton flaring of TeV blazars III. Linear and nonlinear electron cooling with the full Klein-Nishina cross section", A&A (2008)

Röken, C., Schlickeiser, R., "Nonlinear radiative cooling of relativistic particles under partition conditions III. Multiple instantaneous monoenergetic injections", A&A (2008)

eingereicht worden.

Contents

1	Introduction	1
1.1	Blazars	1
1.2	Elementary radiation processes	3
1.2.1	Synchrotron emission	3
1.2.2	Inverse Compton scattering of internally generated photons	3
1.3	Aim of the thesis	6
2	Synchrotron cooling processes in flaring TeV blazars	7
2.1	Linear and nonlinear electron synchrotron cooling in the case of <i>two</i> instantaneous monoenergetic injections	9
2.2	Linear and nonlinear electron synchrotron cooling in the case of <i>multiple</i> instantaneous monoenergetic injections	12
2.3	Intrinsic optically thin synchrotron radiation	13
2.3.1	Optically thin synchrotron intensities	13
2.3.2	Optically thin synchrotron fluences	20
2.4	Discussion	23
3	Synchrotron self-Compton radiation process	25
3.1	Nonlinear synchrotron self-Compton emission in the δ -distribution approximation	26
3.1.1	Intrinsic synchrotron radiation formulas	26
3.1.2	Synchrotron radiation intensities	28
3.1.3	Synchrotron photon density distribution	29
3.1.4	Synchrotron self-Compton emission	29
3.1.5	Synchrotron self-Compton fluences	31
3.2	Linear and nonlinear synchrotron self-Compton emission with the full Klein-Nishina cross section	36

3.2.1	Linear and nonlinear synchrotron self-Compton intensities	36
3.2.2	Linear and nonlinear synchrotron self-Compton fluences	41
3.3	Discussion	50
4	Summary and Conclusions	53
A	Single electron differential scattering rate	55
B	Solution of the electron kinetic equation with two injections for linear cooling	59
C	Solution of the electron kinetic equation with two injections for nonlinear cooling	61
C.1	The case $\xi \gg 1$	63
C.2	The case $\xi \ll 1$	66
D	Optically thin synchrotron radiation intensities	67
E	Synchrotron optical depth and photon spectra	69
E.1	Optical depth	69
E.2	Synchrotron spectra	70
	Bibliography	73

1 Introduction

1.1 Blazars

In this thesis we examine internal radiation processes of extragalactic objects called blazars. In a nutshell, as a member of the group of the active galactic nuclei (Schlick-eiser, 2002) a blazar is a very compact, supermassive astrophysical entity. It is characterised by a strong short-time energy variability (non-thermal spectrum ranging from very low radio frequencies to high-energy γ -rays) of the flares in its relativistic jets in the order of days with a high degree of polarization. The apparent compactness and rapid energy variability of blazars is a consequence of the particular angle of observation since the jet is pointing in the general direction of the Earth, so that we observe (nearly) downward the jet. Blazars can be divided into two groups

Group 1: Highly variable quasars or so-called Optically Violent Variable quasars

Group 2: BL Lacertae (BL Lac) objects

There are a few objects that exhibit a mixture of properties from both blazar groups designated intermediate blazars. It is assumed that Optically Violent Variable quasars are intrinsically powerful radio galaxies, whereas BL Lacertae objects are intrinsically weak radio galaxies (Xie et al., 1993). The host galaxies with presumed central supermassive black holes are giant ellipticals for both group 1 and group 2. The name "blazar" emerged from the combination of these two groups.

Like in the standard scenario for all active galactic nuclei (Antonucci, 1993), blazars are expected to be powered by various matter, e.g. gas and dust, spirally falling into the central black hole of the host galaxy. Due to this process a hot accretion disc of size $\sim 10^{-3}$ parsecs generating immense amounts of energy arises. This energy is transferred to electromagnetic radiation and several elementary particles, e.g. electrons and positrons. A highly energetic plasma in the form of discrete plasmoids (usually a

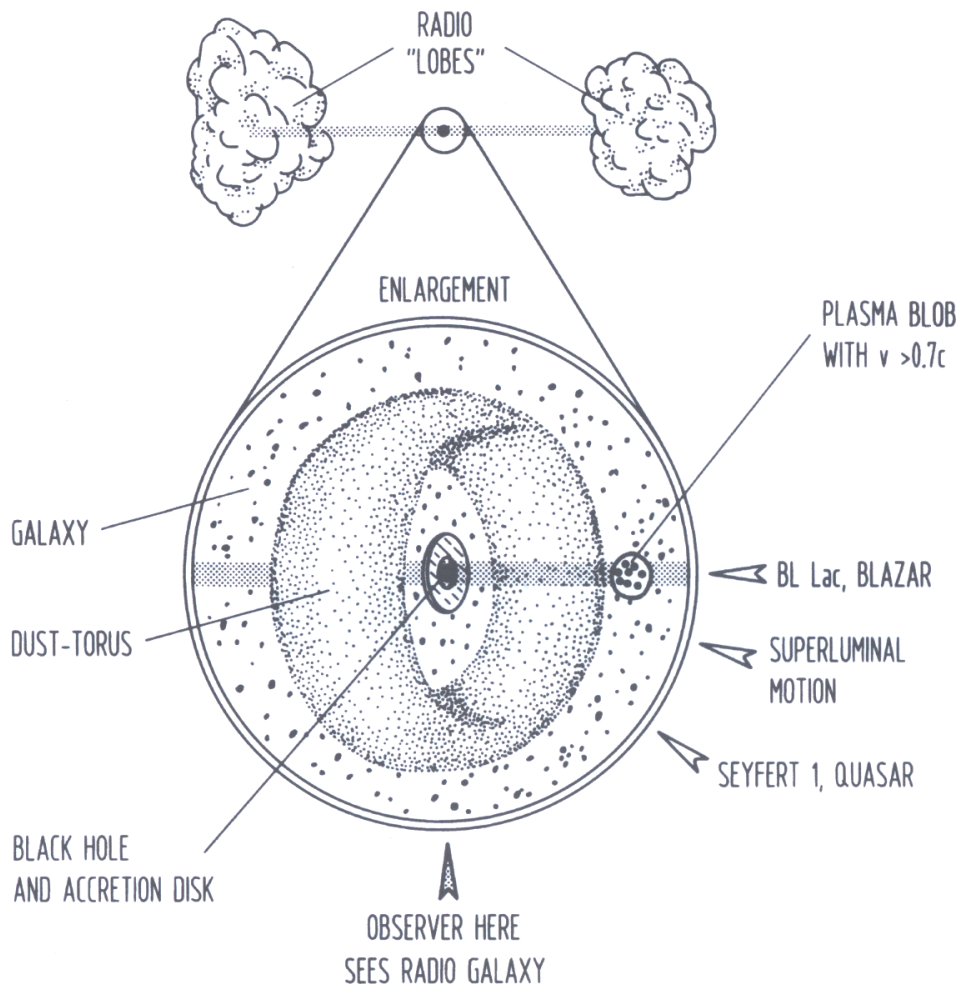


Figure 1.1: Schematic model of the outer part of an active galactic nuclei jet system extracted from Schlickeiser (2002).

proton-electron plasma) is transported away from the blazar in a pair of relativistic jets expanding over tens of kiloparsecs, perpendicular to the accretion disc from the central black hole. Strong magnetic fields and exceeding winds produced by the accretion disc and the opaque torus of hot gas localized several parsecs away from the black hole (see Figure 1.1) lead to a collimation of the jets.

Interactions between high-energy photons, relativistic particles and the strong magnetic fields within the plasmoids produce the observed synchrotron radiation in the radio to X-ray spectrum and inverse Compton radiation in the X-ray to γ -ray range. The origins of the high-energy photons and particles, the nature of the interactions as well as the configuration of the magnetic fields are specified in the introductions of Chapters 2 and 3.

Blazars show a huge enhancement of the observed emission in their jets due to relativistic effects (relativistic aberration, time dilation) called relativistic beaming (Ghisellini et al., 1993) and an apparent superluminal characteristic within the first few parsecs of their jets (Mutel et al., 1990). Here, we apply theoretical emission models with standard linear and recently introduced nonlinear electron synchrotron cooling (Schlickeiser and Lerche, 2007) to blazars radiating in the high-energy γ -ray regime. These objects are called TeV-blazars. Famous members are for example Markarian 421, Markarian 501 and PKS 2155-304.

1.2 Elementary radiation processes

1.2.1 Synchrotron emission

A part of the blazar radiation emission model considered in Chapter 3 is a synchrotron self-Compton emission model based on the assumption that internally created synchrotron radiation is inverse Compton scattered to higher energies by its generating electron population. Synchrotron radiation is a form of electromagnetic radiation produced by the acceleration of relativistic, charged particles in magnetic fields. Here, we consider only the synchrotron emission of relativistic electrons and positrons. A detailed discussion of synchrotron emission including the necessary synchrotron radiation formulas is provided in Chapters 2.3.1 and 3.1.1. In Figure 1.2 we show the observed multi-wavelength spectrum of the blazar Markarian 421. The low-energy peak is related to the synchrotron radiation, while the high-energy peak is assigned to the synchrotron self-Compton or inverse Compton scattering process.

1.2.2 Inverse Compton scattering of internally generated photons

The differential inverse Compton scattering rate, \dot{n}_s , in a coordinate system comoving with the radiation source (unprimed quantities) is given by Dermer et al. (1992)

$$\dot{n}_s(\epsilon_s, \Omega_s) = \int_1^\infty \oint n_e(\gamma, \Omega_e) \frac{d^3 N}{dt d\Omega_s d\epsilon_s} d\Omega_e d\gamma, \quad (1.1)$$

where γ is the normalised energy of a single electron, ϵ_s the normalised energy of a scattered photon, N the scattered photon number, n_e the differential electron density

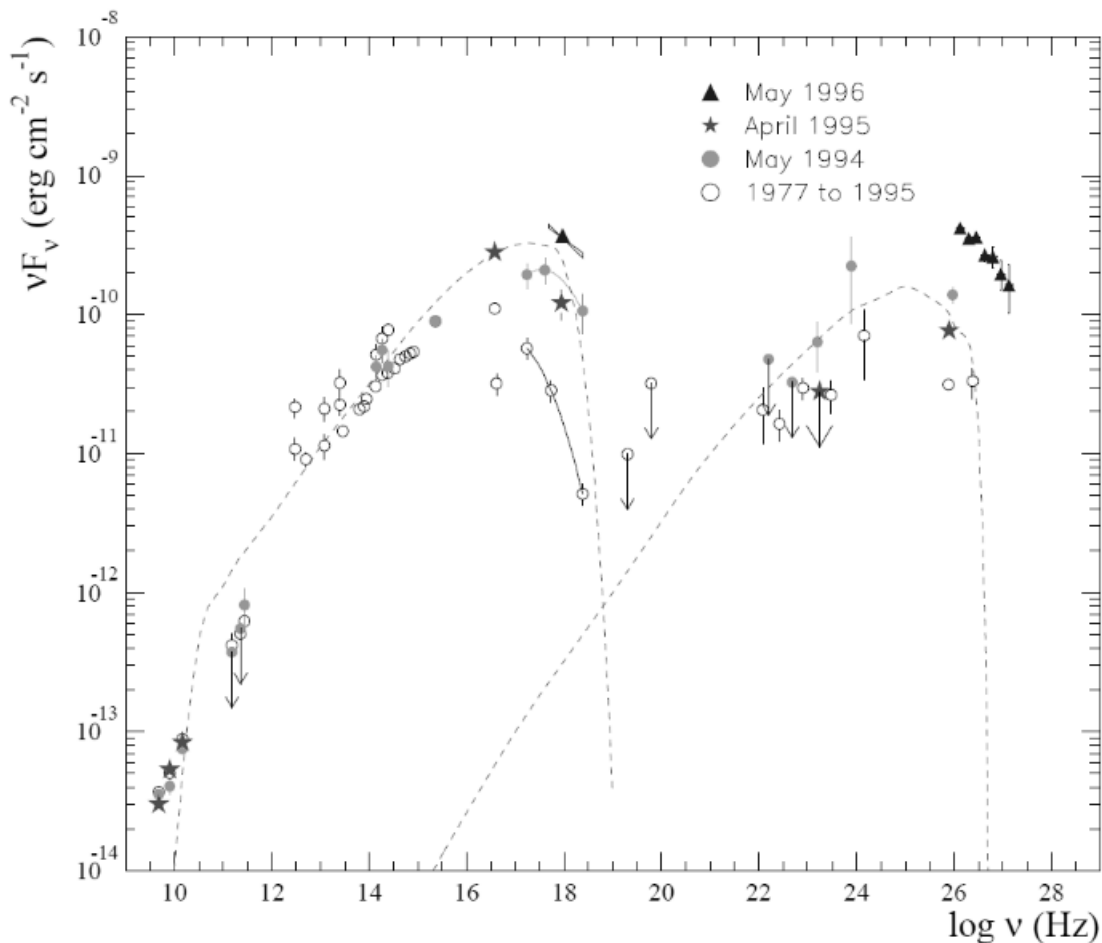


Figure 1.2: The multi-wavelength power spectrum of Markarian 421 extracted from T.C. Weekes (2000) showing a low-energy peak related to synchrotron radiation and a high-energy peak assigned to the synchrotron self-Compton process.

and Ω_s and Ω_e are the solid angles of the scattered photons and electrons, respectively. The single electron differential scattering rate reads

$$\frac{d^3 N}{dt d\Omega_s d\epsilon_s} = c \int_0^\infty \oint (1 - \beta \cos \psi) n(\epsilon, \Omega) \frac{d^2 \sigma}{d\epsilon_s d\Omega_s} d\Omega d\epsilon \quad (1.2)$$

with the normalised energy of an incoming photon ϵ , the differential synchrotron photon density n and $\psi = \angle(\vec{v}_e, \vec{k}_{ph})$. \vec{v}_e is the velocity of the electron and \vec{k}_{ph} is the wave vector of the incoming photon. The differential Klein-Nishina cross section, $d^2 \sigma / (d\epsilon_s d\Omega_s)$, is on the one hand implemented in its Thomson limit (Chapter 3.1) via a δ -distribution approximation (Dermer and Schlickeiser, 1993)

$$\dot{n}_s(\epsilon_s, \tau) = \frac{c\sigma_T}{3\pi} \int_0^\infty n(\epsilon, \tau) \int_1^{1/\epsilon} n_e(\gamma, \tau) \delta(\epsilon_s - \gamma^2 \epsilon) d\gamma d\epsilon \quad (1.3)$$

and otherwise to its full extent (Chapter 3.2). There, it has the most compact form in the rest frame of the electrons (primed quantities) (Jauch and Rohrlich, 1976)

$$\frac{d^2\sigma}{d\epsilon'_s d\Omega'_s} = \frac{r_0^2}{2} \cdot \frac{\epsilon_s'^2}{\epsilon'^2} \left(\frac{\epsilon'}{\epsilon'_s} + \frac{\epsilon'_s}{\epsilon'} - \sin^2 \chi' \right) \delta(\epsilon'_s - \epsilon'_0), \quad (1.4)$$

where

$$\epsilon'_0 = \frac{\epsilon'}{1 + \epsilon'(1 - \cos \chi')} \quad (1.5)$$

and $\chi = \angle(\vec{k}_s, \vec{k}_{ph})$ with the wave vector \vec{k}_s of the scattered photon. We assume isotropic electron and photon distributions in the comoving frame. Hence, the differential Compton scattering rate does not depend on the direction of the outgoing photons, so that (1.1) can be reduced to

$$\dot{n}_s(\epsilon_s) = \int_1^\infty n_e(\gamma) \frac{d^2N}{dt d\epsilon_s} d\gamma. \quad (1.6)$$

Following the work by Arbeiter et al. (2005) we can write

$$\begin{aligned} \frac{d^2N}{dt d\epsilon_s} &\simeq \frac{\pi r_0^2 c}{2\gamma^2 \epsilon_s} \int_0^\infty \frac{n(\epsilon)}{\epsilon^2} \int_0^\infty \int_{-1}^1 \delta(\epsilon'_s - \epsilon'_0) H\left(\epsilon' - \frac{\epsilon}{2\gamma}\right) H(2\gamma\epsilon - \epsilon') \\ &\quad \cdot \frac{\epsilon_s'^3}{\epsilon'} \left(\frac{\epsilon'}{\epsilon'_s} + \frac{\epsilon'_s}{\epsilon'} - \sin^2 \chi' \right) d\cos \chi' d\epsilon' d\epsilon, \end{aligned} \quad (1.7)$$

where $H(\cdot)$ denotes the Heaviside step function. Using the so-called head-on approximation (Arbeiter, 2005) and $\epsilon_s = \gamma\epsilon'_s(1 - \beta \cos \chi')$ we obtain for the high-energy regime $\epsilon \ll \epsilon_s \leq 4\epsilon\gamma^2/(1 + 4\epsilon\gamma)$ (Blumenthal and Gould, 1970; Jones, 1967)

$$\begin{aligned} \frac{d^2N}{dt d\epsilon_s} &\simeq \frac{2\pi r_0^2 c}{\gamma^2} \int_0^\infty \frac{n(\epsilon)}{\epsilon} H(1 - \Lambda(\epsilon, \epsilon_s)) H(\epsilon_s - \epsilon) \\ &\quad \cdot \left((1 - \Lambda(\epsilon, \epsilon_s)) \left(1 + 2\Lambda(\epsilon, \epsilon_s) [1 + \epsilon_s \epsilon] \right) + 2\Lambda(\epsilon, \epsilon_s) \ln(\Lambda(\epsilon, \epsilon_s)) \right) d\epsilon, \end{aligned} \quad (1.8)$$

with $\Lambda(\epsilon, \epsilon_s) = \epsilon_s / (4\gamma^2\epsilon(1 - \epsilon_s/\gamma))$, and for the low-energy regime $\epsilon/4\gamma^2 \leq \epsilon_s \ll \epsilon$

$$\frac{d^2N}{dt d\epsilon_s} \approx \frac{\pi r_0^2 c}{2\gamma^4} \int_0^\infty \frac{n(\epsilon)}{\epsilon} \left(\frac{4\gamma^2\epsilon_s}{\epsilon} - 1 \right) d\epsilon. \quad (1.9)$$

The detailed calculations can be found in Appendix A. In the following discussion of the synchrotron self-Compton intensities and fluences we use only the *dominating* contribution (1.8) of the differential scattering rate for a single electron and neglect (1.9).

1.3 Aim of the thesis

Blazar emission models include, in general, various processes that are responsible for the creation of or have an influence on the radiation, e.g. cooling processes, diffusion, collisions or injections (perturbations). The aim of this thesis is to investigate a new nonlinear electron synchrotron cooling behaviour due to an assumed partition condition between the energy density of the ambient magnetic field and that of the relativistic electrons in the plasmoids.

This nonlinear cooling behaviour is very distinct from the *standard* linear electron cooling because of the consideration of the time-dependence of the magnetic field, which has a massive influence on the evolution of the electrons. Therefore, we solve the electron kinetic differential equation for the linear as well as for the nonlinear electron synchrotron cooling in the case of multiple instantaneous injections of mono-energetic ultra-relativistic electrons. Afterwards, we apply the obtained solutions to the synchrotron self-Compton process in a δ -distribution approximation and compare the results with an actual time-averaged blazar spectrum to determine the quality of the models in comparison to each other. To generalise these results we also analytically compute the synchrotron self-Compton emissions without making use of approximations, i.e. with the full Klein-Nishina cross section.

2 Synchrotron cooling processes in flaring TeV blazars

A field of current activity in theoretical astroparticle physics represents the modelling of the broadband photon spectra of non-thermal radiation sources (e.g. blazars) showing two broad spectral components (see Figure 1.2). The quantitative reproduction of the detected spectra is exceptionally successful using homogeneous one-zone models (Mastichiadis and Kirk, 2002) under simplified assumptions for relativistically propagating regions of emission in the jets of active galactic nuclei. In this work we discuss such a model and its applicability.

The first step in initialising such a model is to set up physical assumptions about the origin of the low-energy and high-energy components of the spectra. It is generally accepted that the low-energy component consists of non-thermal radiation from high-energy relativistic electrons (Böttcher, 2007), where synchrotron radiation is favoured. The high-energy component is assumed to be created by inverse Compton emission (Chapter 3). In addition to the synchrotron radiation model for the low-energy spectral component, other propositions such as electrostatic bremsstrahlung (Schlickeiser, 2003) or Jitter radiation (Medvedev et al., 2007; Workman et al., 2008) are discussed.

All these models have in common that the evolving energy distribution of the radiating particles (electrons) is determined by a time-dependent kinetic equation for the volume-averaged relativistic electron population in the plasmoid (Kardashev, 1962), governing the competition between the injection, escape and energy loss processes. Here, we assume electron energy losses in form of a synchrotron cooling with a constant magnetic field B (standard linear electron synchrotron cooling) on the one hand and on the other a partition condition between the energy densities of the magnetic field ($U_B(t) = B(t)^2/8\pi$) and the relativistic electrons

$$U_e(t) = m_e c^2 \int_0^\infty \gamma N(p, t) dp \quad (2.1)$$

(nonlinear electron synchrotron cooling), first introduced by Schlickeiser and Lerche (2007) and expressed by a constant partition parameter $e_B = U_B(t)/U_e(t)$. This approach appears reasonable because particle-in-cell simulations of the observed spectral energy distributions (Böttcher and Chiang, 2002; Dermer and Schlickeiser, 2002) provide the best results in agreement to the experimental data (e.g. Aharonian et al., 2006, 2007) if a partition condition is assumed although there is no obvious physical justification for this behaviour. However, the success of this assumption in explaining the observational findings when modelling the spectra of active galactic nuclei vindicates its application. Hence, the magnetic field strength becomes time-dependent, $B(t) = \sqrt{8\pi e_B U_e(t)}$, adopting itself to the actual kinetic energy density of the radiating electrons in these sources, leading to twofold consequences:

1. Focusing only on the synchrotron radiation of relativistic electrons the energy loss rate depends on the kinetic energy density of the radiating particles, which is an integral over the electron differential spectral density (2.1). The synchrotron radiation cooling of the relativistic electrons shows, thus, *nonlinear* behaviour. We could consider the synchrotron radiation of heavier charged particles such as hadrons (Reimer et al., 2004) and muons (Böttcher and Reimer, 2004), the Thomson cross section of hadrons of charge Ze and mass Am_p $\sigma_H = Z^4 m_e^2 \sigma_T / A^2 m_p^2 = 2.96 \cdot 10^{-7} \sigma_T$ is, however, six orders of magnitude smaller than the electron Thomson cross section $\sigma_T = 6.65 \cdot 10^{-25} \text{cm}^2$ and therefore, we can neglect this contribution.
2. The synchrotron photon emissivity and fluence will be modified as compared to the standard case of a constant magnetic field.

This magnetic field is most likely generated from the interaction of the relativistically moving emission knot (plasmoid) with the ambient interstellar and intergalactic mediums that are also responsible for the injection of the ultra-relativistic particles by the relativistic pick-up process (Gerbig and Schlickeiser, 2007; Pohl and Schlickeiser,

2000; Stockem et al., 2007). Further information regarding the relativistic collisions of plasma shells can be found in Frederiksen et al. (2004), Jaroschek et al. (2005), Kapetanacos (1974), Lee and Lampe (1973), Ng and Noble (2006), Nishikawa et al. (2003), Sakai et al. (2004), Silva et al. (2003) and Tatarakis et al. (2003).

The nonlinear cooling effect was discussed and compared to the linear cooling process in Schlickeiser and Lerche (2007, 2008) for the cases of *one* instantaneous injection of monoenergetic ultra-relativistic electrons and an instantaneous injection of *power-law* distributed electrons. In Chapters 2.1 and 2.2 we consider, for the first time, the cases of *two* and *multiple* instantaneous injections of monoenergetic ultra-relativistic electrons, respectively. We calculate in detail all necessary physical quantities for *two* injections with strengths q_0 and q_1 at times t_0 and t_1 . It can be shown that asymptotic analytical solutions can only be found for four or less injections, so that numerical methods have to be applied for a number of injections ≥ 5 . The necessity of discussing multiple injections into a physical system where partition conditions hold is obvious: why should nature stop at one injection?

This chapter is structured as follows: First, we solve the basic time-dependent volume-averaged kinetic equations for the linear ($U_B = \text{const.}, B = \text{const.}$) and the nonlinear ($U_B = U_B(t), B = B(t)$) case. Second, we derive the time-dependent synchrotron radiation spectra and synchrotron fluences for both cases and finally examine extensively the obtained differences. All necessary mathematical details can be found in Appendices B and C.

2.1 Linear and nonlinear electron synchrotron cooling in the case of two instantaneous monoenergetic injections

In the following, a comoving coordinate system is chosen for the discussion of the linear and nonlinear cooling processes of relativistic electrons in the interior of the radiation source due to synchrotron radiation in a large-scale magnetic field of random orientation.

Two competitive processes govern the intrinsic evolution of the plasmoid. The instantaneous injection of ultra-relativistic electrons $\gamma_k \gg 1$ at the rate $Q(\gamma_k, t)$, where γ_k is the electron energy of the k -th injection, and the electron synchrotron losses. Kardashev (1962) derived a partial differential equation describing the time-dependent evolution of the volume-averaged relativistic electron population inside such a radiating source

$$\frac{\partial n(\gamma, t)}{\partial t} - \frac{\partial}{\partial \gamma} (|\dot{\gamma}| n(\gamma, t)) = Q(\gamma, t), \quad (2.2)$$

where $n(\gamma, t)$ is the volume-averaged differential number density, $|\dot{\gamma}| = D_0 \gamma^2$ the energy loss rate responsible for the electron cooling and $D_0 = 4\sigma_T / (3m_e c) \cdot U_B$. Assuming the electrons to be ultra-relativistic ($\gamma \gg 1$) for all times, the relation $p \simeq m_e c \gamma$ holds, implying the connection $N(p, t) = n(\gamma, t) / m_e c$ between the particular differential electron number densities leading to an energy integrated kinetic energy density of the relativistic electrons $U_e(t) = m_e c^2 \int_0^\infty \gamma n(\gamma, t) d\gamma$.

Suppose that two monoenergetic injections occur at times t_0 and t_1 at the rate

$$Q(\gamma, t) = q_0 \delta(\gamma - \gamma_0) \delta(t - t_0) + q_1 \delta(\gamma - \gamma_1) \delta(t - t_1), \quad (2.3)$$

the solution of the kinetic equation (2.2) in the case of linear cooling, i.e. for a constant energy density U_B , resulting in a constant D_0 , reads in the different time regimes (Appendix B)

$$n_L(\gamma, t | t_0 \leq t < t_1) = q_0 H(\gamma_0 - \gamma) \delta(\gamma - \gamma_L^{(0)}(t)) \quad (2.4)$$

and

$$n_L(\gamma, t | t_0 < t_1 \leq t) = q_0 H(\gamma_0 - \gamma) \delta(\gamma - \gamma_L^{(0)}(t)) + q_1 H(\gamma_1 - \gamma) \delta(\gamma - \gamma_L^{(1)}(t)), \quad (2.5)$$

respectively, where

$$\gamma_L^{(k)}(t) = \frac{\gamma_k}{1 + D_0 \gamma_k (t - t_k)} \quad (2.6)$$

denotes the time-dependent linear electron Lorentz factors with $k = 0, 1$.

The nonlinear case is based on the assumption of partition, i.e. the magnetic field energy density $U_B(t) = e_B U_e(t) = e_B m_e c^2 \int_0^\infty \gamma n(\gamma, t) d\gamma$ depends on an energy integral of the actual electron spectrum. Therefore, the energy loss rate is $|\dot{\gamma}| = A_0 \gamma^2 \int_0^\infty \gamma n(\gamma, t) d\gamma$ with the abbreviation $A_0 = 4c\sigma_T e_B/3$. The solutions for the kinetic equation in the two time regimes yield (Appendix C)

$$n_{NL}(\gamma, t | t_0 \leq t < t_1) = q_0 H(\gamma_0 - \gamma) \delta(\gamma - \gamma_{NL}) \quad (2.7)$$

and

$$n_{NL}(\gamma, t | t_0 < t_1 \leq t) = q_0 H(\gamma_0 - \gamma) \delta(\gamma - \gamma_{NL}^{(0)}) + q_1 H(\gamma_1 - \gamma) \delta(\gamma - \gamma_{NL}^{(1)}) \quad (2.8)$$

with

$$\gamma_{NL} = \frac{\gamma_0}{\sqrt{1 + 2q_0 A_0 \gamma_0^2 (t - t_0)}} \quad (2.9)$$

and

$$\begin{aligned} \gamma_{NL}^{(k)} = & \gamma_0 \gamma_1 \left(\sqrt{2q A_0 \gamma_0^2 \gamma_1^2 (t - t_1) + \left(\hat{q}_1 \gamma_0 + \hat{q}_0 \gamma_1 \sqrt{2q_0 A_0 \gamma_0^2 (t_1 - t_0) + 1} \right)^2} \right. \\ & \left. + (-1)^k \hat{q}_{|k-1|} \left(\gamma_1 \sqrt{2q_0 A_0 \gamma_0^2 (t_1 - t_0) + 1} - \gamma_0 \right) \right)^{-1}, \end{aligned} \quad (2.10)$$

where $q \equiv q_0 + q_1$ and $\hat{q}_k \equiv q_k/q$. As we can see from (2.10) the two injections are coupled in the nonlinear cooling case due to the time dependence of the magnetic field energy density. We will examine this particular behaviour in the following sections. The results of the linear and nonlinear electron synchrotron cooling in the case of *one* instantaneous monoenergetic injection $Q(\gamma, t) = q_0 \delta(\gamma - \gamma_0) \delta(t - t_0)$ discussed in Schlickeiser and Lerche (2007) can be trivially reproduced by setting $q_1 = 0$.

2.2 Linear and nonlinear electron synchrotron cooling in the case of multiple instantaneous monoenergetic injections

For $m + 1$ injections the kinetic equation (2.2) reads for the linear cooling case

$$\frac{\partial n(\gamma, t)}{\partial t} - D_0 \frac{\partial}{\partial \gamma} (\gamma^2 n(\gamma, t)) = \sum_{k=0}^m q_k \delta(\gamma - \gamma_k) \delta(t - t_k), \quad (2.11)$$

yielding for the time domain $t_{m-1} < t_m \leq t$ the generalised solution

$$n_L(\gamma, t) = \sum_{k=0}^m q_k H(\gamma_k - \gamma) \delta(\gamma - \gamma_L^{(k)}), \quad m \in \mathbb{N}, \quad (2.12)$$

which is simply a superposition of the single-injection solutions.

In the nonlinear case, the successively injected electron populations have a strong impact on each other due to the significant time- and injection-number-dependence of the magnetic field (see Chapter 2.3.1), so that the gyrofrequency $\nu_0(t)$ (Appendix D) describes coupled states of the Lorentz factors (2.10) leading to a generalised differential equation of the function $T(\tau)$ (see Appendix C), where $\tau = A_0 t$ is a new time variable

$$\frac{dT}{d\tau} = \sum_{k=0}^m q_k \frac{H(T - T(\tau_k))}{T - T(\tau_k) + x_k}, \quad (2.13)$$

yielding for the domain $\tau_{m-1} < \tau_m \leq \tau$ the indefinite integral

$$\int \frac{\prod_{k=0}^m (T - T(\tau_k) + x_k)}{\sum_{k=0}^m \frac{q_k}{T - T(\tau_k) + x_k} \prod_{l=0}^m (T - T(\tau_l) + x_l)} dT = \tau + \text{const.} \quad (2.14)$$

For each value m a different transcendental equation for T solving the integral follows, therefore, no general expression for T and hence, for the density function $n(\gamma, t)$ can be found analytically. Additionally, a limit for reasonable analytical approximate solutions is reached with systems containing four instantaneous monoenergetic injections

because systems with injections ≥ 5 implicate polynomials of degree ≥ 5 in T with undetermined coefficients (see Appendix C) where roots cannot be found analytically, as shown already by Abel (1826). Thus, solutions have to be found numerically for $m \geq 4$ injections. Analytical solutions for $m = 2$ and $m = 3$ can be calculated similar to the case of two injections ($m = 1$) presented in the above subsection.

2.3 Intrinsic optically thin synchrotron radiation

2.3.1 Optically thin synchrotron intensities

We investigate the differences between *single* and *multiple* instantaneous injections of monoenergetic electrons. Therefore, it is sufficient to examine only the regime of optically thin radiation. The description of the optically thick contribution works analogous.

The optically thin synchrotron intensity I from relativistic electrons in a homogeneous source of radius R is (Chapter 3.1.1)

$$I(\nu, t) = \frac{R}{4\pi} \int_0^\infty n(\gamma, t) P(\nu, \gamma) d\gamma, \quad (2.15)$$

where $n(\gamma, t)$ is the volume-averaged differential particle density and

$$P(\nu, \gamma) = P_0 \frac{\nu}{\gamma^2} CS\left(\frac{2\nu}{3\nu_0\gamma^2}\right) \quad (2.16)$$

the pitch-angle averaged synchrotron power of a single electron (Crusius and Schlickeiser, 1986, 1988) with $P_0 = 8.763 \cdot 10^{-29}$ erg and the electron gyrofrequency $\nu_0 = eB/(2\pi m_e c)$. The function $CS(z)$ can be approximated by the expression

$$CS(z) \simeq z^{-2/3} \left(0.869 + z^{1/3} \exp(z) \right)^{-1}. \quad (2.17)$$

Using the results derived in Chapter 2.1 and 2.2 we obtain for the optically thin synchrotron intensities for the linear and nonlinear case each for the domains $t_0 \leq t < t_1$ and $t_0 < t_1 \leq t$

$$I_L(f_L, t_L | t_{L,0} \leq t_L < t_{L,1}) / I_{L,0} = \frac{q_0}{\gamma_0^2} f_L (1 + t_L - t_{L,0})^2 CS\left(f_L (1 + t_L - t_{L,0})^2\right) \quad (2.18)$$

and

$$I_L(f_L, t_L | t_{L,0} < t_{L,1} \leq t_L) / I_{L,0} = \frac{f_L}{\gamma_0^2} \cdot \left[q_0 (1 + t_L - t_{L,0})^2 CS\left(f_L (1 + t_L - t_{L,0})^2\right) + q_1 \left(\frac{\gamma_0}{\gamma_1} + t_L - t_{L,1}\right)^2 CS\left(f_L \left[\frac{\gamma_0}{\gamma_1} + t_L - t_{L,1}\right]^2\right) \right] \quad (2.19)$$

as well as

$$I_{NL}(f_{NL}, t_{NL} | t_{NL,0} \leq t_{NL} < t_{NL,1}) / I_{NL,0} = \frac{q_0}{\gamma_0^2} f_{NL} (1 + t_{NL} - t_{NL,0}) \cdot CS\left(f_{NL} (1 + t_{NL} - t_{NL,0})^{5/4}\right) \quad (2.20)$$

and

$$I_{NL}(f_{NL}, t_{NL} | t_{NL,0} < t_{NL,1} \leq t_{NL}) / I_{NL,0} = f_{NL} \cdot \left[q_0 \gamma_{NL}^{(0)-2}(t_{NL}) \cdot CS\left(\frac{\nu}{\nu_{NL}^{(0)}(t_{NL})}\right) + q_1 \gamma_{NL}^{(1)-2}(t_{NL}) \cdot CS\left(\frac{\nu}{\nu_{NL}^{(1)}(t_{NL})}\right) \right] \quad (2.21)$$

with $I_{L,0} \equiv RP_0 \nu_{L|t=t_0} / (4\pi)$, $I_{NL,0} \equiv RP_0 \nu_{NL|t=t_0} / 4\pi$, the frequencies $f_L = \nu / \nu_{L|t=t_0}$ and $f_{NL} = \nu / \nu_{NL|t=t_0}$, the times $t_L = D_0 \gamma_0 t$ and $t_{NL} = 2q_0 A_0 \gamma_0^2 t$ and the characteristic nonlinear frequencies $\nu_{NL}^{(k)}$ as functions of the characteristic nonlinear Lorentz factors (2.10) (see formula (D.5)).

In Figures 2.1 and 2.2, we show the synchrotron light curves for two injections for the linear and the nonlinear case with a variation in the injection times of the second injection $t_{L,1}$ and $t_{NL,1}$ while the frequencies f_L and f_{NL} remain at one constant value.

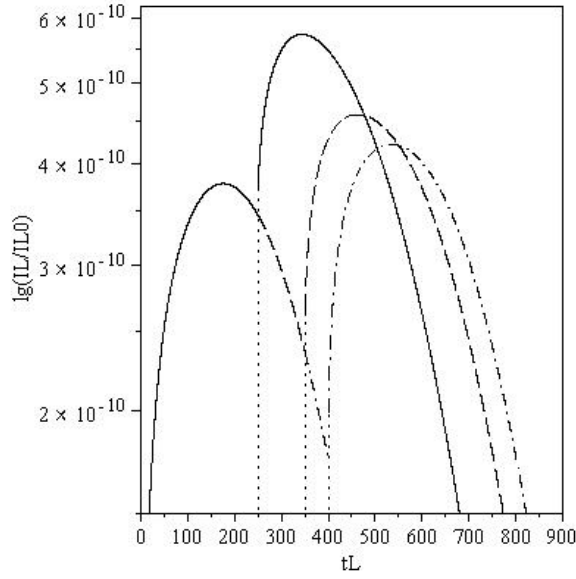


Figure 2.1: Normalised synchrotron light curves $I_L/I_{L,0}$ as functions of the time t_L in the linear cooling case at the frequency $f_L = 10^{-5}$ for three second injection times $t_{L,1} = 250$ (solid curve), $t_{L,1} = 350$ (dashed curve & solid curve for $t_L < 250$) and $t_{L,1} = 400$ (dash-dotted curve & dashed curve for $250 \leq t_L < 350$ & solid curve for $t_L < 250$).

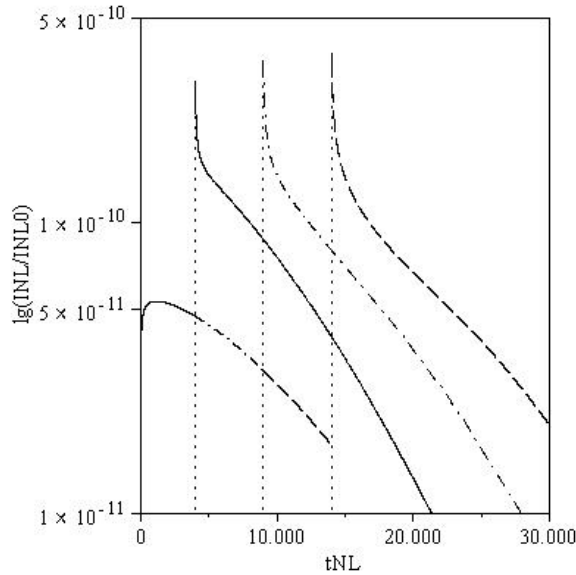


Figure 2.2: Normalised synchrotron light curves $I_{NL}/I_{NL,0}$ as functions of the time t_{NL} in the nonlinear cooling case at the frequency $f_{NL} = 10^{-5}$ for three second injection times $t_{NL,1} = 4000$ (solid curve), $t_{NL,1} = 9000$ (dash-dotted curve & solid curve for $t_{NL} < 4000$) and $t_{NL,1} = 14000$ (dashed curve & dash-dotted curve for $4000 \leq t_{NL} < 9000$ & solid curve for $t_{NL} < 4000$).

The first injection occurs at $t_0 = 0$ with $q_0 = q_1 = 10^5$ and $\gamma_0 = \gamma_1 = 10^7$ in all figures. In the linear case we can recognise the simple superposition of the independent Green's-solutions (2.19) due to the constancy of the magnetic field throughout all times going from the domain of the first injection $t_0 \leq t < t_1$ to the domain $t_0 < t_1 \leq t$ governed by both injections.

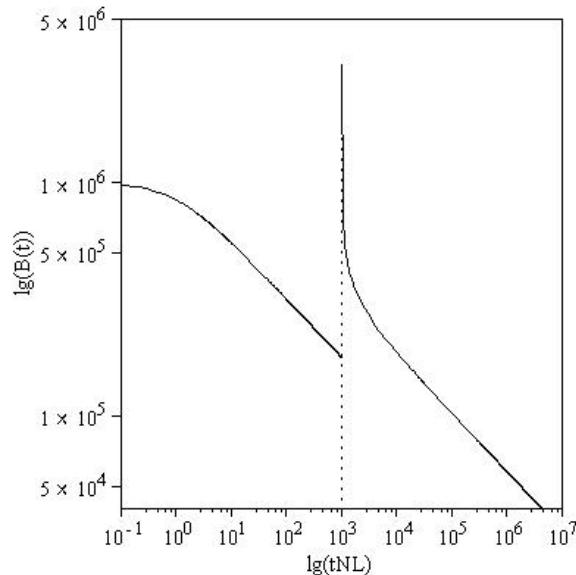


Figure 2.3: Normalised magnetic field $B(t)/B_0$ as a function of the time t_{NL} in the nonlinear cooling case for the second injection time $t_{NL,1} = 1000$.

In contrast, the magnetic field for the nonlinear cooling depends on time as well as the number, strength and energy of injections as shown in Figure 2.3 for $t_{NL,1} = 1000$. Here, the magnetic field discontinuously peaks when the second injection takes place because of the coupling of the nonlinear characteristic Lorentz factors (2.10) in the second domain

$$B(t_0 \leq t < t_1) = B_0 \left(\int_0^\infty \gamma n(\gamma, t) d\gamma \right)^{1/2} = B_0 \sqrt{q_0 \gamma_{NL}} \quad (2.22)$$

$$B(t_0 < t_1 \leq t) = B_0 \sqrt{q_0 \gamma_{NL}^{(0)} + q_1 \gamma_{NL}^{(1)}},$$

where $B_0 \equiv c\sqrt{8\pi m_e e_B}$, explaining the behaviour of the functions in Figure 2.2.

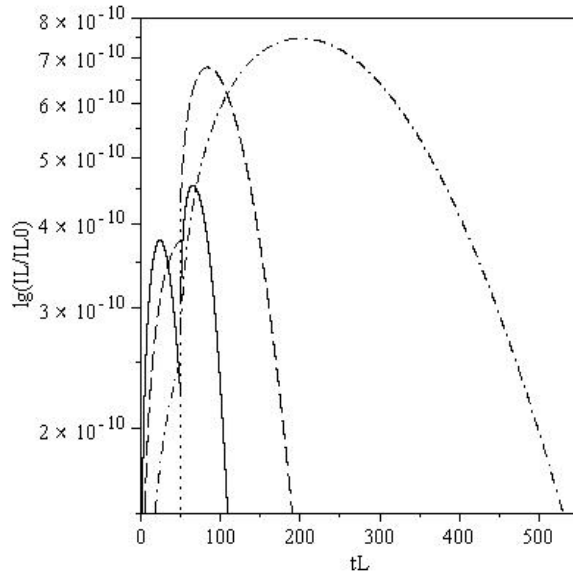


Figure 2.4: Normalised synchrotron light curves $I_L/I_{L,0}$ as functions of the time t_L in the linear cooling case at three different frequencies $f_L = 10^{-5}$ (dash-dotted curve), $f_L = 10^{-4}$ (dashed curve) and $f_L = 5 \cdot 10^{-4}$ (solid curve) for the second injection time $t_{L,1} = 50$.

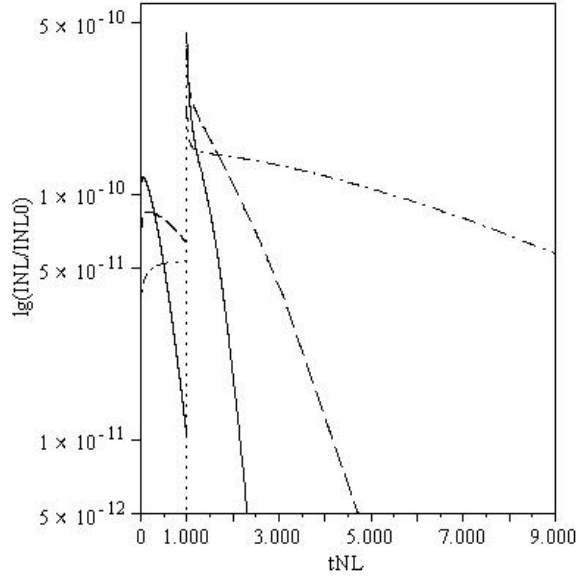


Figure 2.5: Normalised synchrotron light curves $I_{NL}/I_{NL,0}$ as functions of the time t_{NL} in the nonlinear cooling case at three different frequencies $f_{NL} = 10^{-5}$ (dash-dotted curve), $f_{NL} = 10^{-4}$ (dashed curve) and $f_{NL} = 5 \cdot 10^{-4}$ (solid curve) for the second injection time $t_{NL,1} = 1000$.

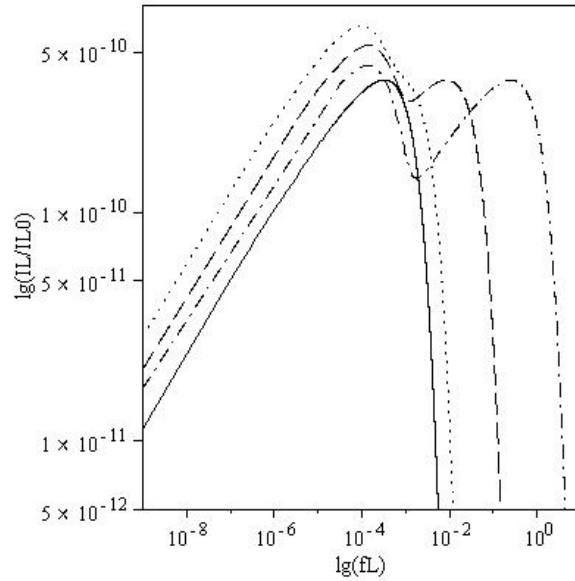


Figure 2.6: Synchrotron intensity $I_L/I_{L,0}$ as a function of the frequency f_L in the linear cooling case at four different times $t_L = 30$ (solid curve), $t_L = 50.1$ (dash-dotted curve), $t_L = 55$ (dashed curve) and $t_L = 70$ (dotted curve). The second injection occurs at $t_{L,1} = 50$.

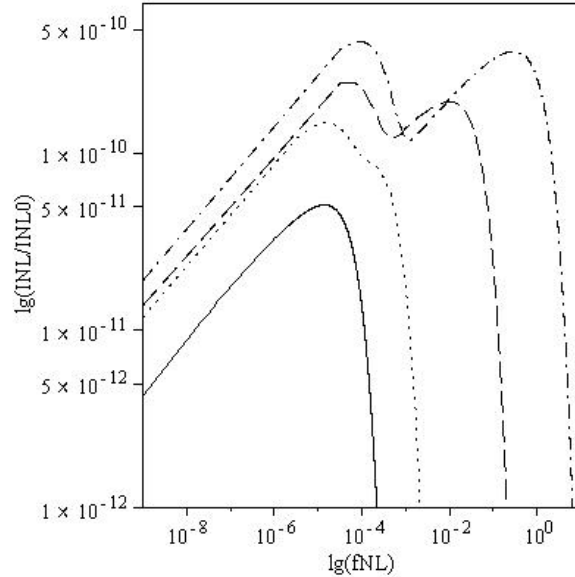


Figure 2.7: Synchrotron intensity $I_{NL}/I_{NL,0}$ as a function of the frequency f_{NL} in the nonlinear cooling case at four different times $t_{NL} = 3000$ (solid curve), $t_{NL} = 4001$ (dash-dotted curve), $t_{NL} = 4100$ (dashed curve) and $t_{NL} = 5000$ (dotted curve). The second injection occurs at $t_{NL,1} = 4000$.

The synchrotron light curves for fixed second injection times but different frequencies are presented in Figures 2.4 and 2.5. In Figures 2.6 and 2.7, we display the synchrotron spectra for both cooling cases at different times t_L and t_{NL} , whereas a second injection occurs at times $t_{L,1} = 50$ and $t_{NL,1} = 4000$. In the two diagrams the spectra each show a low-frequency and a high-frequency maximum shortly after the second injection (dash-dotted and dashed curves) noticeable in the crossing-regions of the zoomed-in light curves in Figure 2.8 exemplified for the linear cooling case.

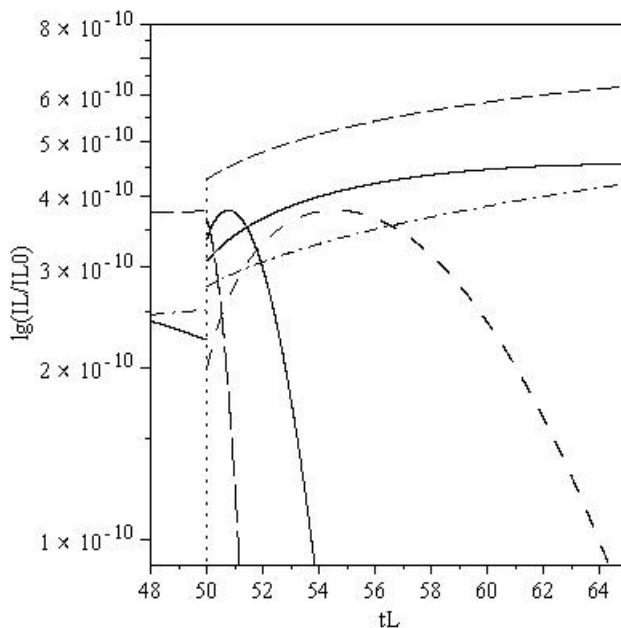


Figure 2.8: Normalised synchrotron light curves $I_L/I_{L,0}$ as functions of the time t_L in the linear cooling case *in the vicinity of the time of the second injection* $t_{L,1} = 50$ at six different frequencies $f_L = 10^{-5}$ (dash-dotted curve), $f_L = 10^{-4}$ (dashed curve), $f_L = 5 \cdot 10^{-4}$ (solid curve), $f_L = 10^{-2}$ (space-dashed curve), $f_L = 10^{-1}$ (solid curve with stronger curvature) and $f_L = 5 \cdot 10^{-1}$ (long-dashed curve).

For later times the spectra (dotted curves) converge against the low-frequency maximum form of a one-injection spectrum (solid curves) because the high-frequency maximum is shifted to lower frequencies and additionally it decreases for the nonlinear case more rapid in time than the low-frequency maximum. As one can see, the particles already being present in a system with nonlinear cooling are emitting higher energetic synchrotron radiation due to the increase in magnetic field energy while the new par-

ticles are entering the system. This does not happen in the linear cooling case because the magnetic field is constant during the second injection.

2.3.2 Optically thin synchrotron fluences

The time-integrated synchrotron fluence

$$F(\nu) = \int_{t_0}^{\infty} I(\nu, t) dt \quad (2.23)$$

has to be split into two integrals over the specified injection time-domains each for the linear and nonlinear cooling cases

$$F(\nu) = \int_{t_0}^{t_1} I(\nu, t | t_0 \leq t < t_1) dt + \int_{t_1}^{\infty} I(\nu, t | t_0 < t_1 \leq t) dt. \quad (2.24)$$

The fluence for the linear electron cooling then reads

$$\begin{aligned} F_L(\nu) &= H_0 \left[q_0 \int_{t_0}^{t_1} \frac{\nu}{\nu_L^{(0)}} CS\left(\frac{\nu}{\nu_L^{(0)}}\right) dt + \int_{t_1}^{\infty} \left(q_0 \frac{\nu}{\nu_L^{(0)}} CS\left(\frac{\nu}{\nu_L^{(0)}}\right) + q_1 \frac{\nu}{\nu_L^{(1)}} CS\left(\frac{\nu}{\nu_L^{(1)}}\right) \right) dt \right] \\ &= H_0 \left[q_0 \int_{t_0}^{\infty} \frac{\nu}{\nu_L^{(0)}} CS\left(\frac{\nu}{\nu_L^{(0)}}\right) dt + q_1 \int_{t_1}^{\infty} \frac{\nu}{\nu_L^{(1)}} CS\left(\frac{\nu}{\nu_L^{(1)}}\right) dt \right] \end{aligned} \quad (2.25)$$

using (2.18) and (2.19) with $H_0 \equiv 3RP_0\nu_0/(8\pi)$. Transforming dt into $d\nu_L^{(k)}$ leads to the expression

$$\begin{aligned} F_L(\nu) &= \frac{H'_0}{\nu^{3/2}} \left[q_0 \int_0^{\nu_L^{(0)} |_{t=t_0}} \left(\frac{\nu}{\nu_L^{(0)}}\right)^{5/2} CS\left(\frac{\nu}{\nu_L^{(0)}}\right) d\nu_L^{(0)} \right. \\ &\quad \left. + q_1 \int_0^{\nu_L^{(1)} |_{t=t_1}} \left(\frac{\nu}{\nu_L^{(1)}}\right)^{5/2} CS\left(\frac{\nu}{\nu_L^{(1)}}\right) d\nu_L^{(1)} \right]. \end{aligned} \quad (2.26)$$

Substituting $f_L^{(k)} = \nu/\nu_L^{(k)}$ the fluence yields

$$F_L(\nu) = \frac{F_{L,0}}{\nu^{1/2}} \left[q_0 \int_{f_L^{(0)}|_{t=t_0}}^{\infty} f_L^{(0)1/2} CS(f_L^{(0)}) df_L^{(0)} + q_1 \int_{f_L^{(1)}|_{t=t_1}}^{\infty} f_L^{(1)1/2} CS(f_L^{(1)}) df_L^{(1)} \right], \quad (2.27)$$

where $F_{L,0} \equiv \sqrt{3\nu_0} H_0 / (2^{3/2} D_0)$. Here, we use the asymptotic expansion of the function (2.17)

$$CS(z) \simeq \begin{cases} a_0 z^{-2/3} & , z \ll 1 \\ z^{-1} \exp(-z) & , z \gg 1 \end{cases} \quad (2.28)$$

with $a_0 = 1.151$ to derive the asymptotic behaviour of the fluence integrals for low and high frequencies ν . The calculations for these integrals are analogous to the calculations of Schlickeiser and Lerche (2007) due to the superposition of the *single* instantaneous monoenergetic injection character of the linear solution (2.5). For low frequencies $\nu \ll 1$ we obtain

$$F_L(\nu \ll 1) = \frac{F_{L,0}}{\nu^{1/2}} \left[q_0 \left(c_0 - \frac{6a_0}{5} (f_L^{(0)}|_{t=t_0})^{5/6} \right) + q_1 \left(c_0 - \frac{6a_0}{5} (f_L^{(1)}|_{t=t_1})^{5/6} \right) \right], \quad (2.29)$$

where $c_0 = 0.866$. In the high-frequency range $\nu \gg 1$ we get

$$F_L(\nu \gg 1) = \frac{F_{L,0}}{\nu^{1/2}} \left[q_0 (f_L^{(0)}|_{t=t_0})^{-1/2} \exp(-f_L^{(0)}|_{t=t_0}) + q_1 (f_L^{(1)}|_{t=t_1})^{-1/2} \exp(-f_L^{(1)}|_{t=t_1}) \right]. \quad (2.30)$$

With the intensities (2.20) and (2.21) the nonlinear fluence yields immediately

$$F_{NL}(\nu) = \frac{RP_0\nu}{4\pi} \left[\int_{t_0}^{t_1} q_0 \gamma_{NL}^{-2} CS\left(\frac{\nu}{\nu_{NL}}\right) dt + \int_{t_1}^{\infty} \left(q_0 \gamma_{NL}^{(0)-2} CS\left(\frac{\nu}{\nu_{NL}^{(0)}}\right) + q_1 \gamma_{NL}^{(1)-2} CS\left(\frac{\nu}{\nu_{NL}^{(1)}}\right) \right) dt \right]. \quad (2.31)$$

The first integral gives after similar substitutions

$$F_{NL}(\nu) = \frac{F_{NL,0}}{\nu^{3/5}} \int_{f_{NL|t=t_0}}^{f_{NL|t=t_1}} f_{NL}^{3/5} CS(f_{NL}) df_{NL}, \quad (2.32)$$

where $F_{NL,0} \equiv RP_0/(5\pi A_0) \cdot (3c\sqrt{2e_B r_0 q_0/\pi}/2)^{8/5}$. We find for the asymptotic frequency regimes

$$F_{NL}(\nu \ll 1) = \frac{15a_0 F_{NL,0}}{14\nu^{3/5}} \left(f_{NL|t=t_1} - f_{NL|t=t_0} \right) \quad (2.33)$$

and

$$\begin{aligned} F_{NL}(\nu \gg 1) &= \frac{F_{NL,0}}{\nu^{3/5}} \Gamma\left(\frac{3}{5}, f_{NL|t=t_0}, f_{NL|t=t_1}\right) \\ &\approx \frac{F_{NL,0}}{\nu^{3/5}} \left(f_{NL|t=t_0}^{-2/5} \exp\left[-f_{NL|t=t_0}\right] - f_{NL|t=t_1}^{-2/5} \exp\left[-f_{NL|t=t_1}\right] \right). \end{aligned} \quad (2.34)$$

To solve the second integral of (2.31) we introduce a new time-variable

$$\omega = \sqrt{\omega_0(t - t_1) + \omega_1^2} \quad (2.35)$$

with $\omega_0 \equiv 2q\gamma_0^2\gamma_1^2 A_0$ and $\omega_1 \equiv \hat{q}_1\gamma_0 + \hat{q}_0\gamma_1 \cdot \sqrt{2q_0\gamma_0^2 A_0(t_1 - t_0) + 1}$. Additionally we substitute

$$\varkappa_0 \equiv \hat{q}_1 \left(\gamma_1 \sqrt{2q_0\gamma_0^2 A_0(t_1 - t_0) + 1} - \gamma_0 \right) \quad \text{and} \quad \varkappa_1 \equiv -\frac{q_0\varkappa_0}{q_1},$$

so that the characteristic nonlinear Lorentz factors read $\gamma_{NL}^{(k)} = \gamma_0\gamma_1/(\omega + \varkappa_k)$. The fluence then transforms into

$$\begin{aligned} F_{NL}(\nu) &= G_0\nu \int_{\omega_1}^{\infty} \omega \left[q_0(\omega + \varkappa_0)^2 CS\left(\frac{\nu(\omega + \varkappa_0)^2}{\zeta\gamma_0^{5/2}\gamma_1^{5/2}\sqrt{\frac{q_0}{\omega + \varkappa_0} + \frac{q_1}{\omega + \varkappa_1}}}\right) \right. \\ &\quad \left. + q_1(\omega + \varkappa_1)^2 CS\left(\frac{\nu(\omega + \varkappa_1)^2}{\zeta\gamma_0^{5/2}\gamma_1^{5/2}\sqrt{\frac{q_0}{\omega + \varkappa_0} + \frac{q_1}{\omega + \varkappa_1}}}\right) \right] d\omega \end{aligned} \quad (2.36)$$

with $G_0 \equiv RP_0/(2\pi\omega_0\gamma_0^2\gamma_1^2)$ and $\zeta \equiv 3c\sqrt{2e_B r_0/\pi}/2$. To simplify the argument of the function $CS(\cdot)$ we investigate the asymptotes $\omega \ll \varkappa_k$ and $\omega \gg \varkappa_k$. We can assume that $q_0 \approx q_1$ because for $q_k \gg q_{|k-1|}$ we would obtain the case for *one* monoenergetic instantaneous injection. The asymptotic behaviour for $\omega \ll \varkappa_0$ can be omitted since this case does not belong to the domain of integration $\gamma_0 + q_0\varkappa_0/q_1 \leq \omega \leq \infty$. For $\omega \gg \varkappa_0$ (2.36) reduces to

$$F_{NL}(\nu) = \frac{2qG_0}{\omega_0\gamma_0^2\gamma_1^2}\nu \int_{\omega_1}^{\infty} \omega^3 CS\left(\frac{\nu\omega^{5/2}}{\zeta q^{1/2}\gamma_0^{5/2}\gamma_1^{5/2}}\right) d\omega. \quad (2.37)$$

Replacing $\nu\omega^{5/2}/(\zeta q^{1/2}\gamma_0^{5/2}\gamma_1^{5/2}) = y$ the integral (2.37) reads

$$F_{NL}(\nu) = \tilde{F}_{NL,0}\nu^{-3/5} \int_{y_0}^{\infty} y^{3/5} CS(y) dy, \quad (2.38)$$

where $\tilde{F}_{NL,0} \equiv 4\zeta^{8/5}q^{9/5}\gamma_0^2\gamma_1^2G_0/(5\omega_0)$ and $y_0 \equiv y|_{\omega=\omega_1}$. Then we derive for the low-frequency domain $\nu \ll 1$

$$\begin{aligned} F_{NL}(\nu \ll 1) &= \tilde{F}_{NL,0}\nu^{-3/5} \left(\int_0^{\infty} y^{3/5} CS(y) dy - a_0 \int_0^{y_0} y^{-1/15} dy \right) \\ &= \tilde{F}_{NL,0}\nu^{-3/5} \left(0.793 - \frac{15}{14}a_0y_0^{14/15} \right) \approx 0.793\tilde{F}_{NL,0}\nu^{-3/5} \end{aligned} \quad (2.39)$$

and for the high-frequency domain $\nu \gg 1$

$$\begin{aligned} F_{NL}(\nu \gg 1) &= \tilde{F}_{NL,0}\nu^{-3/5} \int_{y_0}^{\infty} y^{-2/5} \exp(-y) dy \\ &= \tilde{F}_{NL,0}\nu^{-3/5} \Gamma\left(\frac{3}{5}, y_0\right) \approx \tilde{F}_{NL,0}\nu^{-3/5} y_0^{-2/5} \exp(-y_0). \end{aligned} \quad (2.40)$$

2.4 Discussion

For powerful cosmic non-thermal radiation sources such as blazars and γ -ray burst sources it is very likely to observe *multiple* injections of ultra-high energy radiating particles in these sources via a relativistic pick-up process (Pohl and Schlickeiser,

2000). Therefore, we generalised the illustrative case of only one instantaneous injection of monoenergetic particles into sources with assumed time-dependent magnetic field strength that adjusts itself to the actual kinetic energy density of the injected relativistic particles (partition condition) discussed in Schlickeiser and Lerche (2007).

We solved the linear and nonlinear kinetic equation for the intrinsic temporal evolution of the relativistic particles each in the domain of the first ($t_0 \leq t < t_1$) and second injection ($t_0 < t_1 \leq t$) in detail for two instantaneous monoenergetic injections and gave a short overview of analytically obtaining solutions for $m + 1$ injections. The solutions of the linear kinetic differential equation in the domain $t_0 < t_1 \leq t$ serve as a simple superposition of Green's functions, while the solutions of the nonlinear equation show a more complex form due to the nonlinear dependence of the synchrotron loss term on an energy integral of the particle number density leading to a magnetic field coupling of both particle injection populations. Then we calculated the corresponding optically thin synchrotron radiation intensities and synchrotron fluences for each cooling case.

We reproduced not only the differences both in the spectral distributions and synchrotron light curves in the domain $t_0 \leq t < t_1$ presented in Schlickeiser and Lerche (2007), we also found further significant differences in the domain $t_0 < t_1 \leq t$, e.g. a sudden increase in the intensity in the nonlinear light curves or a low- and a high-frequency synchrotron maximum in the linear and nonlinear spectral synchrotron distributions instead of only one low-frequency maximum as in the single-injection spectral synchrotron distributions.

This is caused by the dependence of the magnetic field on time as well as on the number of injections. Thus, we demonstrated that the coupling of the magnetic field energy density to the kinetic energy density of the injected particles results in a completely different cooling behaviour compared to sources with a constant magnetic field changing both the synchrotron emissivity and the intrinsic temporal evolution of the relativistic electron energy spectrum especially after the occurrence of a second injection. The predictions of the spectral behaviour as functions of time or frequency provide conclusive tests for the existence of a linear or nonlinear cooling in flaring non-thermal sources like the flaring blazar jet PKS 2155-304 (see Chapter 3.1.5).

3 Synchrotron self-Compton radiation process

A process for the energy loss of ultra-relativistic electrons in cosmic-ray sources named inverse Compton scattering has been considered to be very likely responsible for the production of the high-energy radiation emitted by active galactic nuclei. In this process low-energy photons are scattered to higher energies by relativistic electrons within the jets of the sources. There are several possible external and internal generators for the low-energy photon field like the accretion disc of the central black hole (Dermer et al., 1992; Dermer and Schlickeiser, 1993), the broad-line region (Sikora et al., 1994), dust surrounding the active galactic nuclei (Arbeiter et al., 2002; Blazejowski et al., 2000) or synchrotron radiation produced by the jet itself. In this chapter the process of interest is the inverse Compton scattering of internal synchrotron radiation called synchrotron self-Compton scattering (Maraschi et al., 1992).

Numerical models were applied in most of the studies of the synchrotron self-Compton process, e.g. Böttcher (2007), Chiaberge and Ghisellini (1999), Dermer et al. (1997), Mastichiadis and Kirk (1997) and Sokolov et al. (2004). In this thesis we investigate *analytically* the influence of a *nonlinear* electron synchrotron cooling on the synchrotron self-Compton process following the analysis of the flaring of TeV blazars due to the synchrotron self-Compton process for a linear synchrotron radiation cooling behaviour of the injected electrons (Schlickeiser and Röken, 2008).

Therefore, we assume that a flare of the emission knot occurs at the time $t = t_0$ due to a single uniform instantaneous injection of monoenergetic ultra-relativistic electrons. The emission knot itself moves with a relativistic bulk speed V with respect to an external observer. We model the emission knot as a spherical magnetised, fully ionised plasma cloud of radius R consisting of cold electrons and protons with a uniform density distribution and a randomly oriented large-scale *time-dependent* magnetic field

$B(t)$ that adjusts itself to the actual kinetic energy density of the radiating electrons in these sources, yielding the nonlinear synchrotron radiation cooling behaviour discussed in Chapter 2. The existence of the magnetic field is mandatory for the generation of synchrotron radiation and hence, the synchrotron self-Compton process.

In Schlickeiser and Röken (2008) the synchrotron self-Compton process was applied to a linear electron synchrotron cooling where a δ -distribution approximation (Dermer and Schlickeiser, 1993; Reynolds, 1982) was used for the computation of the inverse Compton scattering rate \dot{n}_s . Here, we determine the *nonlinear* synchrotron self-Compton emission using the same δ -distribution approximation. Afterwards, we compare in Chapter 3.1.5 the linear to the nonlinear model by application on the data record of the PKS 2155-304 flare on MJD 53944.

Most of the calculations of radiation quantities have been based on such rather simple approximations. Hence, another advantage of this thesis is to determine the inverse Compton scattering rate, the synchrotron self-Compton intensities and fluences for the special class of synchrotron photon densities and electron populations discussed in Chapter 2 for the *full Klein-Nishina cross section* and, therefore, in obtaining more general results (Chapter 3.2).

3.1 Nonlinear synchrotron self-Compton emission in the δ -distribution approximation

3.1.1 Intrinsic synchrotron radiation formulas

For practical reasons, we use another approximation for the pitch-angle averaged synchrotron power of a single electron in vacuum than that, which we applied in Chapter 2.3

$$P(\nu, \gamma) = P_0 \nu_s W\left(\frac{\nu}{\nu_s \gamma^2}\right), \quad (3.1)$$

as well as another definition of the gyrofrequency $\nu_s = 3eB(t)/(4\pi m_e c)$. The function $W(\nu/(\nu_s \gamma^2))$ yields approximately

$$W\left(\frac{\nu}{\nu_s \gamma^2}\right) \simeq a_0 \left(\frac{\nu}{\nu_s \gamma^2}\right)^{1/3} \exp\left(-\frac{\nu}{\nu_s \gamma^2}\right), \quad (3.2)$$

exhibiting a similar asymptotic behaviour as the function $CS(\cdot)$ defined in (2.17) and, therefore, it appears appropriate to use it for the calculations of the intrinsic synchrotron radiation formulas.

In the nonlinear cooling case the gyrofrequency is a time-dependent function due to the imposed partition condition between the energy densities of the magnetic field and the relativistic electrons leading to a time-dependence of the magnetic field

$$B(t) = \sqrt{8\pi e_B U_e} = c\sqrt{8\pi e_B m_e q_0 \gamma_{NL}(t)}. \quad (3.3)$$

Hence, we obtain for the gyrofrequency

$$\nu_s = \nu_0 (1 + \tau - \tau_0)^{-1/4}, \quad (3.4)$$

where $\nu_0 \equiv 3e\sqrt{e_B q_0 \gamma_0 / (2\pi m_e)}$. The synchrotron intensity from relativistic electrons expressed by the volume-averaged differential density $n(\gamma, t)$ for a homogeneous source of radius R reads

$$I(\nu, t) = \frac{j(\nu, t)R}{D(\nu, t)} \left(1 - \exp(-D(\nu, t))\right) \simeq \begin{cases} j(\nu, t)R & , D(\nu, t) \leq 1 \\ \frac{j(\nu, t)R}{D(\nu, t)} & , D(\nu, t) > 1 \end{cases} \quad (3.5)$$

depending on the spontaneous synchrotron emission coefficient

$$j(\nu, t) = \frac{1}{4\pi} \int_0^\infty n(\gamma, t) P(\nu, \gamma) d\gamma = \frac{a_0 P_0 \nu_s^{2/3} \nu^{1/3}}{4\pi} \int_0^\infty n(\gamma, t) \gamma^{-2/3} \exp\left(-\frac{\nu}{\nu_s \gamma^2}\right) d\gamma \quad (3.6)$$

and the synchrotron optical depth, $D(\nu, t) = \mu(\nu, t)R$, where $\mu(\nu, t)$ is the synchrotron absorption coefficient,

$$\begin{aligned}
 D(\nu, t) &= \frac{R}{8\pi m_e \nu^2} \int_0^\infty \frac{n(\gamma, t)}{\gamma^2} \frac{d}{d\gamma} \left(\gamma^2 P(\nu, \gamma) \right) d\gamma \\
 &= \frac{a_0 P_0 R \nu_s^{2/3}}{6\pi m_e \nu^{5/3}} \int_0^\infty n(\gamma, t) \gamma^{-5/3} \left(1 + \frac{3\nu}{2\nu_s \gamma^2} \right) \exp\left(-\frac{\nu}{\nu_s \gamma^2} \right) d\gamma.
 \end{aligned} \tag{3.7}$$

In a strict sense the approximations in (3.5) are valid only for the cases $D(\nu, t) \ll 1$ and $D(\nu, t) \gg 1$. We use, however, an analytic continuation of the approximated synchrotron intensity in order to cover the whole $D(\nu, t)$ -space. This approximation is justified because the calculations shown in Chapters 3.1.4 and 3.1.5 indicate its accuracy.

3.1.2 Synchrotron radiation intensities

Inserting the nonlinear electron density distribution (2.7) into the synchrotron emissivities (3.6) and (3.7) and carrying out the γ -integrations, we obtain in terms of the normalised frequency $\omega = \nu/(\nu_0 \gamma_0^2)$

$$j(\omega, \tau) = \frac{a_0 P_0 q_0 \nu_0}{4\pi} \omega^{1/3} (1 + \tau - \tau_0)^{1/6} \exp\left(-\omega(1 + \tau - \tau_0)^{5/4} \right) \tag{3.8}$$

and

$$D(\omega, \tau) = \left(\frac{\omega_1}{\omega} \right)^{5/3} (1 + \tau - \tau_0)^{2/3} \left(1 + \frac{3}{2} \omega (1 + \tau - \tau_0)^{5/4} \right) \exp\left(-\omega(1 + \tau - \tau_0)^{5/4} \right), \tag{3.9}$$

where we used the characteristic frequency

$$\omega_1 \equiv \left(\frac{a_0 P_0 q_0 R}{6\pi m_e \nu_0 \gamma_0^5} \right)^{3/5}. \tag{3.10}$$

3.1.3 Synchrotron photon density distribution

With the synchrotron intensities (E.6), (E.7) and the definition $\epsilon_0 \equiv h\nu_0\gamma_0^2/(m_e c^2)$ we obtain for the differential synchrotron photon number density

$$n(\epsilon, \tau) = \frac{4\pi}{hc\epsilon} I\left(\frac{\epsilon}{\epsilon_0}, t\right) \quad (3.11)$$

for the case of optically thin energies

$$n(\epsilon > \epsilon_t, \tau) = \frac{4\pi I_0}{hc\epsilon_0^{1/3} \epsilon^{2/3}} (1 + \tau - \tau_0)^{1/6} \exp\left(-\frac{\epsilon}{\epsilon_0} (1 + \tau - \tau_0)^{5/4}\right) \quad (3.12)$$

and for optically thick energies

$$n(\epsilon \leq \epsilon_t, \tau) = \frac{4\pi I_0 \epsilon}{hc\epsilon_0^2 \omega_1^{5/3}} (1 + \tau - \tau_0)^{-1/2} \left(1 + \frac{3\epsilon}{2\epsilon_0} (1 + \tau - \tau_0)^{5/4}\right)^{-1}, \quad (3.13)$$

where $\epsilon_t = \epsilon_0 \omega_t$ is the transition energy from the optically thin to the optically thick synchrotron emission regime. The time variation of the transition frequency ω_t and the synchrotron intensity I can be found in Appendix E.

3.1.4 Synchrotron self-Compton emission

The differential number density of Compton scattered synchrotron photons in the δ -distribution approximation is given by (1.3). The limit imposed on the γ -integral restricts the scattering to the Thomson regime. Here, we neglect effects due to stimulated synchrotron self-Compton emission and absorption leading to the synchrotron self-Compton intensity

$$I_c(\epsilon_s, \tau) = R j_c(\epsilon_s, \tau) = \frac{hR\epsilon_s}{4\pi} \dot{n}_c(\epsilon_s, \tau). \quad (3.14)$$

Inserting the relativistic electron distribution (2.7) into equation (1.3) we obtain

$$\dot{n}_c(\epsilon_s, \tau) = \frac{c\sigma_T q_0}{3\pi\gamma_0^2} (1 + \tau - \tau_0) H\left(\frac{\gamma_0}{\sqrt{1 + \tau - \tau_0}} - \epsilon_s\right) n\left(\frac{\epsilon_s(1 + \tau - \tau_0)}{\gamma_0^2}, \tau\right). \quad (3.15)$$

Equation (3.14) then yields

$$I_c(\epsilon_s, \tau) = \frac{c\sigma_T h R q_0 \epsilon_s}{12\pi^2 \gamma_0^2} (1 + \tau - \tau_0) H\left(\frac{\gamma_0}{\sqrt{1 + \tau - \tau_0}} - \epsilon_s\right) n\left(\frac{\epsilon_s(1 + \tau - \tau_0)}{\gamma_0^2}, \tau\right). \quad (3.16)$$

Making use of the synchrotron photon number densities (3.12) and (3.13) we find for the synchrotron self-Compton intensity

$$I_c\left(\epsilon_s \leq \frac{\epsilon_t \gamma_0^2}{1 + \tau - \tau_0}, \tau\right) = \frac{R\sigma_T q_0 I_0}{3\pi\gamma_0^4 \epsilon_0^2 \omega_1^{5/3}} \epsilon_s^2 (1 + \tau - \tau_0)^{3/2} H\left(\frac{\gamma_0}{\sqrt{1 + \tau - \tau_0}} - \epsilon_s\right) \cdot \left[1 + \frac{3}{2} \frac{\epsilon_s}{\epsilon_0 \gamma_0^2} (1 + \tau - \tau_0)^{9/4}\right]^{-1} \quad (3.17)$$

and

$$I_c\left(\epsilon_s > \frac{\epsilon_t \gamma_0^2}{1 + \tau - \tau_0}, \tau\right) = \frac{R\sigma_T q_0 I_0}{3\pi\gamma_0^{2/3} \epsilon_0^{1/3}} \epsilon_s^{1/3} (1 + \tau - \tau_0)^{1/2} H\left(\frac{\gamma_0}{\sqrt{1 + \tau - \tau_0}} - \epsilon_s\right) \cdot \exp\left(-\frac{\epsilon_s(1 + \tau - \tau_0)^{9/4}}{\epsilon_0 \gamma_0^2}\right), \quad (3.18)$$

respectively.

We introduce a strictly increasing function to simplify later expressions and relations

$$\epsilon_k(\tau) = \frac{\epsilon_t(\tau) \gamma_0^2}{1 + \tau - \tau_0}. \quad (3.19)$$

For times $\tau - \tau_0$ less and greater than $\omega_1^{-20/33} \equiv \tau_1$ (see Appendix E) we obtain, continuing analytically the τ -domain,

$$\epsilon_k(\tau - \tau_0 \leq \tau_1) = \frac{\epsilon_0 \omega_1 \gamma_0^2}{(1 + \tau - \tau_0)^{3/5}} \quad (3.20)$$

and

$$\epsilon_k(\tau - \tau_0 > \tau_1) = \frac{\epsilon_0 \gamma_0^2}{(\tau - \tau_0)^{9/4}} \ln\left(\frac{3}{2} \omega_1^{5/3} (\tau - \tau_0)^{11/4}\right), \quad (3.21)$$

respectively, using equations (E.2) and (E.5).

3.1.5 Synchrotron self-Compton fluences

We discuss the synchrotron self-Compton fluence distribution described by the time-integrated synchrotron self-Compton intensity (3.14)

$$F(\epsilon_s) = \int_{t_0}^{\infty} I_c(\epsilon_s, t) dt = \frac{1}{2A_0 q_0 \gamma_0^2} \int_{\tau_0}^{\infty} I_c^{NL}(\epsilon_s, \tau) d\tau \quad (3.22)$$

in two scattered photon energy ranges: for energies $\epsilon_s > \epsilon_k(\tau_0) = \epsilon_{k,max}$ only the optically thin synchrotron photon distribution (3.18) contributes, whereas at lower energies $\epsilon_s \leq \epsilon_k(\tau_0) = \epsilon_{k,max}$ both the optically thin and thick parts (3.17) and (3.18) of the synchrotron photon distribution have to be taken into account.

High scattered photon energies

For energies $\epsilon_s > \epsilon_k(\tau_0) = \epsilon_{k,max}$ only equation (3.18) contributes, so that

$$F(\epsilon_s > \epsilon_k(\tau_0)) = \frac{R\sigma_T I_0}{6\pi A_0 \gamma_0^{8/3} \epsilon_0^{1/3}} \epsilon_s^{1/3} \int_{\tau_0}^{\infty} (1 + \tau - \tau_0)^{1/2} \exp\left(-\frac{\epsilon_s(1 + \tau - \tau_0)^{9/4}}{\epsilon_0 \gamma_0^2}\right) \cdot H\left(\frac{\gamma_0}{\sqrt{1 + \tau - \tau_0}} - \epsilon_s\right) d\tau. \quad (3.23)$$

Substituting $z = 1 + \tau - \tau_0$ yields

$$F(\epsilon_s > \epsilon_k(\tau_0)) = \frac{F_0 \epsilon_s^{1/3}}{\gamma_0^{13/6} \epsilon_0^{1/3}} \int_1^{(\gamma_0/\epsilon_s)^2} z^{1/2} \exp\left(-\frac{\epsilon_s z^{9/4}}{\epsilon_0 \gamma_0^2}\right) dz, \quad (3.24)$$

where

$$F_0 \equiv \frac{R\sigma_T I_0}{6\pi A_0 \gamma_0^{1/2}}. \quad (3.25)$$

We obtain with the new variable $y = \epsilon_s^2 z / \gamma_0^2$

$$F(\epsilon_s > \epsilon_k(\tau_0)) = \frac{F_0 \gamma_0^{5/6}}{\epsilon_0^{1/3} \epsilon_s^{8/3}} \int_{(\epsilon_s/\gamma_0)^2}^1 y^{1/2} \exp\left(-\frac{\gamma_0^{5/2} y^{9/4}}{\epsilon_0 \epsilon_s^{7/2}}\right) dy. \quad (3.26)$$

Defining $s = y^{9/4}$ and $\epsilon_f \equiv \gamma_0^{5/7}/\epsilon_0^{2/7}$ the fluence reads

$$F(\epsilon_s > \epsilon_k(\tau_0)) = \frac{4F_0\epsilon_f^{7/6}}{9\epsilon_s^{8/3}} \int_{(\epsilon_s/\gamma_0)^{9/2}}^1 s^{-1/3} \exp\left(-\left[\frac{\epsilon_f}{\epsilon_s}\right]^{7/2} s\right) ds. \quad (3.27)$$

For high scattered photon energies $\epsilon_f < \epsilon_s \leq \gamma_0$ the argument of the exponential function in the integral of equation (3.27) becomes very small for all values of s yielding approximately

$$F(\epsilon_s > \epsilon_f > \epsilon_k(\tau_0)) = \frac{4F_0\epsilon_f^{7/6}}{9\epsilon_s^{8/3}} \int_{(\epsilon_s/\gamma_0)^{9/2}}^1 s^{-1/3} ds = \frac{2F_0\epsilon_f^{7/6}}{3\epsilon_s^{8/3}} \left(1 - \left[\frac{\epsilon_s}{\gamma_0}\right]^3\right). \quad (3.28)$$

For scattered photon energies $\epsilon_k(\tau_0) \leq \epsilon_s < \epsilon_f$ we substitute $v = s(\epsilon_f/\epsilon_s)^{7/2}$ to obtain for the fluence (3.27)

$$F(\epsilon_f > \epsilon_s \geq \epsilon_k(\tau_0)) = \frac{4F_0}{9\epsilon_s^{1/3}\epsilon_f^{7/6}} \int_{\epsilon_f^{7/2}\epsilon_s/\gamma_0^{9/2}}^{(\epsilon_f/\epsilon_s)^{7/2}} v^{-1/3} e^{-v} dv = \frac{4F_0}{9\epsilon_s^{1/3}\epsilon_f^{7/6}} \Gamma\left(\frac{2}{3}, \frac{\epsilon_f^{7/2}\epsilon_s}{\gamma_0^{9/2}}, \left[\frac{\epsilon_f}{\epsilon_s}\right]^{7/2}\right) \quad (3.29)$$

in terms of the generalised incomplete gamma function $\Gamma(\cdot, \cdot, \cdot)$. The second argument $\epsilon_f^{7/2}\epsilon_s/\gamma_0^{9/2}$ is much smaller than unity for all scattered photon energies $\epsilon_k(\tau_0) \leq \epsilon_s < \epsilon_f$, while the third argument $(\epsilon_f/\epsilon_s)^{7/2}$ is much larger than unity, so that the generalised incomplete gamma function can be asymptotically expanded (Abramowitz and Stegun, 1972) leading to the approximated fluence distribution

$$F(\epsilon_f > \epsilon_s \geq \epsilon_k(\tau_0)) = \frac{4F_0}{9\epsilon_s^{1/3}\epsilon_f^{7/6}} \Gamma\left(\frac{2}{3}\right). \quad (3.30)$$

Low scattered photon energies

For low scattered photon energies $\epsilon_s \leq \epsilon_k(\tau_0) = \epsilon_{k,max}$ equations (3.17) and (3.18) contribute to the spectral fluence. Starting with the scattered photon range $\epsilon_k(\tau_1) \leq \epsilon_s \leq \epsilon_k(\tau_0)$ we find substituting as before

$$\begin{aligned}
F(\epsilon_k(\tau_1) \leq \epsilon_s \leq \epsilon_k(\tau_0)) &= \frac{1}{2A_0 q_0 \gamma_0^2} \left(\int_{\tau_0}^{\infty} I_c(\epsilon_s \leq \epsilon_k(\tau), \tau) H(\epsilon_k(\tau - \tau_0 \leq \tau_1) - \epsilon_s) d\tau \right. \\
&\quad \left. + \int_{\tau_0}^{\infty} I_c(\epsilon_s > \epsilon_k(\tau), \tau) H(\epsilon_s - \epsilon_k(\tau - \tau_0 \leq \tau_1)) d\tau \right) \\
&= \frac{R\sigma_T I_0}{6\pi A_0 \gamma_0^2} \left(\frac{\epsilon_s^2}{\gamma_0^4 \epsilon_0^2 \omega_1^{5/3}} \int_1^{(\epsilon_0 \omega_1 \gamma_0^2 / \epsilon_s)^{5/3}} z^{3/2} \left[1 + \frac{3\epsilon_s z^{9/4}}{2\gamma_0^2 \epsilon_0} \right]^{-1} dz \right. \\
&\quad \left. + \frac{\epsilon_s^{1/3}}{\gamma_0^{2/3} \epsilon_0^{1/3}} \int_{(\epsilon_0 \omega_1 \gamma_0^2 / \epsilon_s)^{5/3}}^{(\gamma_0 / \epsilon_s)^2} z^{1/2} \exp\left(-\frac{\epsilon_s z^{9/4}}{\gamma_0^2 \epsilon_0}\right) dz \right). \tag{3.31}
\end{aligned}$$

The integrand of the first integral can be approximated within the domain of integration by

$$z^{3/2} \left[1 + \frac{3\epsilon_s}{2\gamma_0^2 \epsilon_0} z^{9/4} \right]^{-1} \approx z^{3/2}. \tag{3.32}$$

Using this approximation and the previous substitutions we obtain for the fluence

$$\begin{aligned}
F(\epsilon_k(\tau_1) \leq \epsilon_s \leq \epsilon_k(\tau_0)) &= \frac{R\sigma_T I_0}{6\pi A_0 \gamma_0^2} \left(\frac{2\epsilon_s^2}{5\gamma_0^4 \epsilon_0^2 \omega_1^{5/3}} \left(\left[\frac{\epsilon_0 \omega_1 \gamma_0^2}{\epsilon_s} \right]^{25/6} - 1 \right) \right. \\
&\quad \left. + \frac{4\epsilon_0^{1/3} \gamma_0^{2/3}}{9\epsilon_s^{1/3}} \Gamma\left(\frac{2}{3}, \frac{\gamma_0^{11/2} \epsilon_0^{11/4} \omega_1^{15/4}}{\epsilon_s^{11/4}}, \left[\frac{\epsilon_f}{\epsilon_s} \right]^{7/2} \right) \right). \tag{3.33}
\end{aligned}$$

The dominating contribution to the fluence represents again synchrotron photons from the optically thin part of the synchrotron spectrum

$$F(\epsilon_k(\tau_1) \leq \epsilon_s \leq \epsilon_k(\tau_0)) = \frac{4F_0}{9\epsilon_s^{1/3} \epsilon_f^{7/6}} \Gamma\left(\frac{2}{3}\right). \tag{3.34}$$

For scattered photon energies $\epsilon_s < \epsilon_k(\tau_1)$ the fluence reads

$$\begin{aligned}
 F(\epsilon_s < \epsilon_k(\tau_1)) = \frac{1}{2A_0 q_0 \gamma_0^2} & \left(\int_{\tau_0}^{\infty} I_c(\epsilon_s \leq \epsilon_k(\tau), \tau) H(\epsilon_k(\tau - \tau_0) > \tau_1 - \epsilon_s) d\tau \right. \\
 & \left. + \int_{\tau_0}^{\infty} I_c(\epsilon_s > \epsilon_k(\tau), \tau) H(\epsilon_s - \epsilon_k(\tau - \tau_0) > \tau_1) d\tau \right).
 \end{aligned}
 \tag{3.35}$$

Using the substitutions and approximations applied before we obtain

$$F(\epsilon_s < \epsilon_k(\tau_1)) = \frac{4F_0}{9\epsilon_s^{1/3} \epsilon_f^{7/6}} \Gamma\left(\frac{2}{3}, 1\right).
 \tag{3.36}$$

Again the contribution representing the optically thick part of the spectrum is negligibly small compared to the contribution representing the optically thin part demonstrating that the fluence distribution $\propto \epsilon_s^{-1/3}$ also holds in the scattered photon energy range $\epsilon_s < \epsilon_k(\tau_1)$.

AIC model selection test

Figure 3.1 shows the linear (dashed curve) and nonlinear (solid curve) fits to the time-averaged spectrum observed from PKS 2155-304 on MJD 53944 (Aharonian et al., 2007). For the generation of these fits we first had to transform the calculated fluence distributions from the comoving frame into the observer frame (asterisked quantities)

$$F^*(\epsilon_s^*) = D^3 F(\epsilon_s) = D^3 F(\epsilon_s^*/D),
 \tag{3.37}$$

followed by the construction of the linear model parametric function

$$F_L^*(\epsilon_s^*) = P_{L,1} \frac{1 - \left(\frac{\epsilon_s^*}{P_{L,2}}\right)^{7/3}}{\epsilon_s^{*1/4} \left(\Gamma\left(\frac{7}{12}\right)^{-1} + \frac{7}{12} \left(\frac{\epsilon_s^*}{P_{L,3}}\right)^{7/4}\right)}
 \tag{3.38}$$

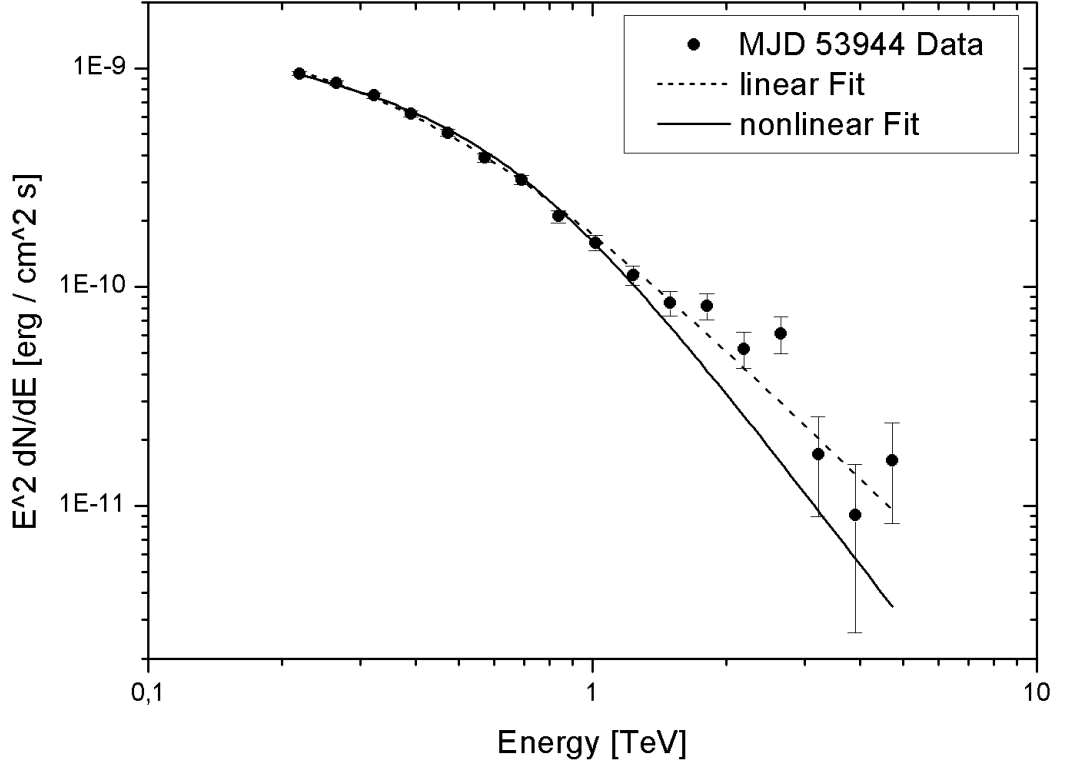


Figure 3.1: Time-averaged spectrum observed from PKS 2155-304 on MJD 53944 (Aharonian et al., 2007). The dashed line represents the fit for the linear cooling case (Schlickeiser and Röken, 2008), whereas the solid curve illustrates the fit for the nonlinear cooling case.

(results from the linear synchrotron self-Compton fluence distribution in the δ -distribution approximation (Schlickeiser and Röken, 2008)) with the parameters $P_{L,1} = D^{11/4} F_0 / \epsilon_f^{3/4}$, $P_{L,2} = D\gamma_0$ and $P_{L,3} = D\epsilon_f$ and the nonlinear model parametric function

$$F_{NL}^*(\epsilon_s^*) = P_{NL,1} \frac{1 - \left(\frac{\epsilon_s^*}{P_{NL,2}}\right)^3}{\epsilon_s^{*1/3} \left(\frac{9}{4} \Gamma\left(\frac{2}{3}\right)^{-1} + \frac{3}{2} \left(\frac{\epsilon_s^*}{P_{NL,3}}\right)^{7/3} \right)} \quad (3.39)$$

with $P_{NL,1} = D^{10/3} F_0 / \epsilon_f^{7/6}$, $P_{NL,2} = D\gamma_0$ and $P_{NL,3} = D\epsilon_f$ from our calculated fluence distributions, which we fitted (3 parameters, 14 degrees of freedom) to the PKS 2155-304 data.

Finally we carried out a so-called AIC model selection test (Akaike, 1974) that measures the quality of a fit of a statistical model, i.e. the precision and complexity of the model, where the preferred model is that with the smallest AIC value. We found the *linear* fit with an AIC value of 13.37 and a reduced χ^2 -value of 1.37 to be more consistent with the data than the nonlinear fit with an AIC value of 30.15 and a reduced χ^2 -value of 3.67. The parameters were determined to be $P_{L,1} = 5.5 \cdot 10^{-10} \pm 1.671 \cdot 10^{-11}$, $P_{L,3} = 0.433 \pm 0.017$ and $P_{NL,1} = 1.007 \cdot 10^{-9} \pm 3.396 \cdot 10^{-11}$, $P_{NL,3} = 0.619 \pm 0.03$. The fits turn out to be independent of the parameters $P_{L,2}$ and $P_{NL,2}$, because both functions (3.38) and (3.39) converge as long as the relation $\epsilon_s^*/P_2 < 1$ is satisfied leading always to the parameters listed above. Note that the test was performed for only *one* specific data record for which the linear fit was found to be the best. To be conclusive, more tests have to be performed.

3.2 Linear and nonlinear synchrotron self-Compton emission with the full Klein-Nishina cross section

3.2.1 Linear and nonlinear synchrotron self-Compton intensities

For the differential scattering rate $\dot{n}_s(\epsilon_s, \tau)$ we use the dominating high-energy contribution (1.8) yielding (see Appendix A)

$$\begin{aligned} \dot{n}_s(\epsilon_s, \Omega_s) = 2\pi r_0^2 c \int_1^\infty \frac{n_e(\gamma)}{\gamma^2} \int_0^\infty \frac{n(\epsilon)}{\epsilon} H(1 - \Lambda(\epsilon, \epsilon_s)) H(\epsilon_s - \epsilon) \\ \cdot \left((1 - \Lambda(\epsilon, \epsilon_s)) \left(1 + 2\Lambda(\epsilon, \epsilon_s) [1 + \epsilon_s \epsilon] \right) + 2\Lambda(\epsilon, \epsilon_s) \ln(\Lambda(\epsilon, \epsilon_s)) \right) d\epsilon d\gamma. \end{aligned} \quad (3.40)$$

Consequently, we have to distinguish between the three cases $\epsilon\Lambda(\epsilon, \epsilon_s) < \epsilon_s < \epsilon_t$, $\epsilon_t < \epsilon\Lambda(\epsilon, \epsilon_s) < \epsilon_s$ and $\epsilon\Lambda(\epsilon, \epsilon_s) < \epsilon_t < \epsilon_s$. For the linear cooling case the transition energy ϵ_t reads (Schlickeiser and Rönken, 2008)

$$\epsilon_t^L = \epsilon_0 \begin{cases} \omega_1^L(1 + \tau) & , \tau \leq (\omega_1^L)^{-1/3} \\ \frac{1}{\tau^2} \ln \left(\frac{3}{2} (\omega_1^L)^{5/3} \tau^5 \right) & , \tau > (\omega_1^L)^{-1/3} \end{cases} \quad (3.41)$$

and for the nonlinear electron cooling case

$$\epsilon_t^{NL} = \epsilon_0 \begin{cases} \omega_1^{NL}(1 + \tau)^{2/5} & , \tau \leq (\omega_1^{NL})^{-20/33} \\ \frac{1}{\tau^{5/4}} \ln \left(\frac{3}{2} (\omega_1^{NL})^{5/3} \tau^{11/4} \right) & , \tau > (\omega_1^{NL})^{-20/33} \end{cases}. \quad (3.42)$$

Here, we discuss only the case $\epsilon_t < \epsilon\Lambda(\epsilon, \epsilon_s) < \epsilon_s$ as explained below in Chapter 3.2.2. Therefore, we define the functions

$$\epsilon_k^L(\tau) = \frac{4\gamma_0^2 \epsilon_0 \omega_1^L}{1 + \tau} \quad (3.43)$$

and

$$\epsilon_k^{NL}(\tau) = \frac{4\gamma_0^2 \epsilon_0 \omega_1^{NL}}{(1 + \tau)^{3/5}} \quad (3.44)$$

with $\omega_1^{L,NL} = (a_0 P_0 q_0 R / (6\pi \nu_{L,NL} m_e \gamma_0^5))^{3/5}$, $\nu_L = 3eB / (4\pi m_e c)$ and $\nu_{NL} = 3e \sqrt{e_B q_0 \gamma_0 / (2\pi m_e)}$.

Linear electron cooling

To compute the linear differential scattering rate we insert the linear differential electron density (Schlickeiser and Lerche, 2007)

$$n_e^L(\gamma) = q_0 H(\gamma_0 - \gamma) \delta\left(\gamma - \frac{\gamma_0}{1 + \tau}\right) \quad (3.45)$$

and the linear synchrotron photon density

$$n^L(\epsilon, \tau) = \frac{4\pi I_0}{hc\epsilon_0^{1/3} \epsilon^{2/3}} (1 + \tau)^{2/3} \exp\left(-\frac{\epsilon}{\epsilon_0} (1 + \tau)^2\right) \quad (3.46)$$

into equation (3.40). Then we obtain

$$\begin{aligned} \dot{n}_s^L(\epsilon_s, \tau) = n_0(1 + \tau)^{8/3} H\left(\frac{\gamma_0}{\epsilon_s} - 1 - \tau\right) \int_{\bar{\Lambda}_L(\epsilon_s, \tau)}^{\epsilon_s} \epsilon^{-5/3} \exp(-f(\tau)\epsilon) \\ \cdot \left((1 - \Lambda_L(\epsilon, \epsilon_s, \tau)) \left(1 + 2\Lambda_L(\epsilon, \epsilon_s, \tau) [1 + \epsilon_s \epsilon] \right) + 2\Lambda_L(\epsilon, \epsilon_s, \tau) \ln(\Lambda_L(\epsilon, \epsilon_s, \tau)) \right) d\epsilon \end{aligned} \quad (3.47)$$

with the constant $n_0 \equiv 8\pi^2 r_0^2 q_0 I_0 / (h\epsilon_0^{1/3} \gamma_0^2)$ and the functions $f(\tau) = (1 + \tau)^2 / \epsilon_0$, $\Lambda_L(\epsilon, \epsilon_s, \tau) = \epsilon_s(1 + \tau)^2 / (4\gamma_0^2 \epsilon (1 - \epsilon_s(1 + \tau) / \gamma_0))$ and $\bar{\Lambda}_L(\epsilon_s, \tau) \equiv \epsilon \Lambda_L(\epsilon, \epsilon_s, \tau)$. Transforming $d\epsilon$ into $d\Lambda_L(\epsilon, \epsilon_s, \tau)$ we find

$$\begin{aligned} \dot{n}_s^L(\epsilon_s, \tau) = n_0(1 + \tau)^{8/3} \bar{\Lambda}_L(\epsilon_s, \tau)^{-2/3} H\left(\frac{\gamma_0}{\epsilon_s} - 1 - \tau\right) \int_{\bar{\Lambda}_L(\epsilon_s, \tau) / \epsilon_s}^1 \Lambda_L(\epsilon, \epsilon_s, \tau)^{-1/3} \\ \cdot \exp\left(-\frac{f(\tau)\bar{\Lambda}_L(\epsilon_s, \tau)}{\Lambda_L(\epsilon, \epsilon_s, \tau)}\right) \left(a_1(\epsilon_s, \tau) + a_2(\epsilon_s, \tau) \Lambda_L(\epsilon, \epsilon_s, \tau) - 2\Lambda_L(\epsilon, \epsilon_s, \tau)^2 \right. \\ \left. + 2\Lambda_L(\epsilon, \epsilon_s, \tau) \ln(\Lambda_L(\epsilon, \epsilon_s, \tau)) \right) d\Lambda_L(\epsilon, \epsilon_s, \tau), \end{aligned} \quad (3.48)$$

where $a_{1/2}(\epsilon_s, \tau) = 1 \pm 2\epsilon_s \bar{\Lambda}_L(\epsilon_s, \tau)$. As shown in Chapter 3.2.2 we expect a change of the intensity and fluence behaviours to occur only at high energies, so that (3.48) is sufficiently well approximated by

$$\begin{aligned} \dot{n}_s^L(\epsilon_s, \tau) \approx n_0(1 + \tau)^{8/3} a_1(\epsilon_s, \tau) \bar{\Lambda}_L(\epsilon_s, \tau)^{-2/3} H\left(\frac{\gamma_0}{\epsilon_s} - 1 - \tau\right) \int_{\bar{\Lambda}_L(\epsilon_s, \tau) / \epsilon_s}^1 \Lambda_L(\epsilon, \epsilon_s, \tau)^{-1/3} \\ \cdot \exp\left(-\frac{f(\tau)\bar{\Lambda}_L(\epsilon_s, \tau)}{\Lambda_L(\epsilon, \epsilon_s, \tau)}\right) (1 - \Lambda_L(\epsilon, \epsilon_s, \tau)) d\Lambda_L(\epsilon, \epsilon_s, \tau). \end{aligned} \quad (3.49)$$

Substituting $s = f(\tau)\bar{\Lambda}_L(\epsilon_s, \tau)\Lambda_L(\epsilon, \epsilon_s, \tau)^{-1}$ we obtain

$$\dot{n}_s^L(\epsilon_s, \tau) = n_0(1 + \tau)^{8/3} a_1(\epsilon_s, \tau) f(\tau)^{2/3} H\left(\frac{\gamma_0}{\epsilon_s} - 1 - \tau\right) \int_{f(\tau)\bar{\Lambda}_L(\epsilon_s, \tau)}^{f(\tau)\epsilon_s} s^{-5/3} e^{-s} \left(1 - \frac{f(\tau)\bar{\Lambda}_L(\epsilon_s, \tau)}{s}\right) ds, \quad (3.50)$$

which is solved by generalised incomplete Gamma functions

$$\begin{aligned} \dot{n}_s^L(\epsilon_s, \tau) &= n_0(1 + \tau)^{8/3} a_1(\epsilon_s, \tau) f(\tau)^{2/3} H\left(\frac{\gamma_0}{\epsilon_s} - 1 - \tau\right) \left[\Gamma\left(-\frac{2}{3}, f(\tau)\bar{\Lambda}_L(\epsilon_s, \tau), f(\tau)\epsilon_s\right) \right. \\ &\quad \left. - f(\tau)\bar{\Lambda}_L(\epsilon_s, \tau) \Gamma\left(-\frac{5}{3}, f(\tau)\bar{\Lambda}_L(\epsilon_s, \tau), f(\tau)\epsilon_s\right) \right] \\ &\approx n_0(1 + \tau)^{8/3} a_1(\epsilon_s, \tau) f(\tau)^{2/3} H\left(\frac{\gamma_0}{\epsilon_s} - 1 - \tau\right) \left[\Gamma\left(-\frac{2}{3}, f(\tau)\bar{\Lambda}_L(\epsilon_s, \tau)\right) \right. \\ &\quad \left. - f(\tau)\bar{\Lambda}_L(\epsilon_s, \tau) \Gamma\left(-\frac{5}{3}, f(\tau)\bar{\Lambda}_L(\epsilon_s, \tau)\right) \right]. \end{aligned} \quad (3.51)$$

We, thus, find the linear synchrotron self-Compton intensity to be

$$\begin{aligned} I_c^L(\epsilon_s, \tau) &= I_0^{KN} \epsilon_s (1 + \tau)^{8/3} a_1(\epsilon_s, \tau) f(\tau)^{2/3} H\left(\frac{\gamma_0}{\epsilon_s} - 1 - \tau\right) \\ &\quad \cdot \left[\Gamma\left(-\frac{2}{3}, f(\tau)\bar{\Lambda}_L(\epsilon_s, \tau)\right) - f(\tau)\bar{\Lambda}_L(\epsilon_s, \tau) \Gamma\left(-\frac{5}{3}, f(\tau)\bar{\Lambda}_L(\epsilon_s, \tau)\right) \right], \end{aligned} \quad (3.52)$$

where $I_0^{KN} \equiv hRn_0/(4\pi)$. In Figures 3.2 and 3.3 we show the linear synchrotron intensity (3.52) as a function of the energy ϵ_s at four different times ($\tau = 0, 10, 10^2, 10^3$) and as a function of the time τ at four different energies ($\epsilon_s = 10^3, 10^4, 10^5, 10^6$).

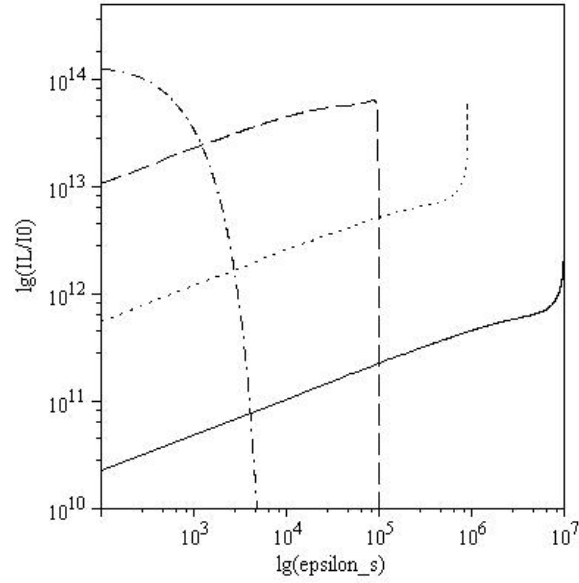


Figure 3.2: Normalised linear synchrotron intensity I_L/I_0 as a function of the energy ϵ_s at four different times $\tau = 0$ (solid curve), 10 (dotted curve), 10^2 (dashed curve) and 10^3 (dash-dotted curve).

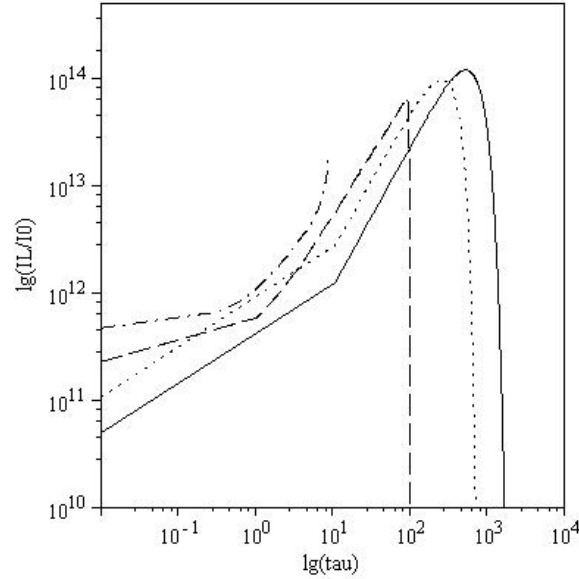


Figure 3.3: Normalised linear synchrotron light curve I_L/I_0 as a function of the time τ at four different energies $\epsilon_s = 10^3$ (solid curve), 10^4 (dotted curve), 10^5 (dashed curve) and 10^6 (dash-dotted curve).

Nonlinear electron cooling

With the nonlinear differential electron density (2.7) and the nonlinear synchrotron photon density (3.12) with $t_0 = 0$ the differential scattering rate reads

$$\begin{aligned} \dot{n}_s^{NL}(\epsilon_s, \tau) \approx n_0(1 + \tau)^{7/6} b_1(\epsilon_s, \tau) g(\tau)^{2/3} H\left(\frac{\gamma_0^2}{\epsilon_s^2} - 1 - \tau\right) \\ \cdot \left[\Gamma\left(-\frac{2}{3}, g(\tau) \bar{\Lambda}_{NL}(\epsilon_s, \tau)\right) - g(\tau) \bar{\Lambda}_{NL}(\epsilon_s, \tau) \Gamma\left(-\frac{5}{3}, g(\tau) \bar{\Lambda}_{NL}(\epsilon_s, \tau)\right) \right], \end{aligned} \quad (3.53)$$

where $g(\tau) = (1 + \tau)^{5/4} / \epsilon_0$, $\bar{\Lambda}_{NL}(\epsilon_s, \tau) = \epsilon_s(1 + \tau) / (4\gamma_0^2(1 - \epsilon_s\sqrt{1 + \tau}/\gamma_0))$ and $b_1(\epsilon_s, \tau) = 1 + 2\epsilon_s \bar{\Lambda}_{NL}(\epsilon_s, \tau)$, applying the same substitutions and approximations as for the linear case. We obtain for the intensity

$$\begin{aligned} I_c^{NL}(\epsilon_s, \tau) = I_0^{KN} \epsilon_s(1 + \tau)^{7/6} b_1(\epsilon_s, \tau) g(\tau)^{2/3} H\left(\frac{\gamma_0^2}{\epsilon_s^2} - 1 - \tau\right) \\ \cdot \left[\Gamma\left(-\frac{2}{3}, g(\tau) \bar{\Lambda}_{NL}(\epsilon_s, \tau)\right) - g(\tau) \bar{\Lambda}_{NL}(\epsilon_s, \tau) \Gamma\left(-\frac{5}{3}, g(\tau) \bar{\Lambda}_{NL}(\epsilon_s, \tau)\right) \right]. \end{aligned} \quad (3.54)$$

In Figures 3.4 and 3.5 we present the nonlinear synchrotron intensity (3.54) as a function of the energy ϵ_s at five different times ($\tau = 0, 10, 10^2, 10^3, 10^5$) and as a function of the time τ at four different energies ($\epsilon_s = 10^3, 10^4, 10^5, 10^6$). The different electron synchrotron cooling behaviours can be well observed by comparing for example Figures 3.2 and 3.4. We can see that the functional behaviour of the linear intensity distribution at $\tau = 10^2$ fits the behaviour of the nonlinear intensity distribution at later times $\tau > 10^2$ due to a faster linear cooling process.

3.2.2 Linear and nonlinear synchrotron self-Compton fluences

Here, we only have to examine the range for high scattered photon energies $\epsilon_s > 4\gamma_0^2 \epsilon_0 \omega_1^{L,NL} = \epsilon_{k,max}^{L,NL}$ because the effect of the *full* Klein-Nishina cross section becomes apparent just in the high-energy scattered photon regime for both the linear and nonlinear case as shown in the following subsections. For energies much lower than a characteristic energy $\epsilon_s < \epsilon_f^{L,NL}$ we find the same solutions as in Chapter 3.1.5 and

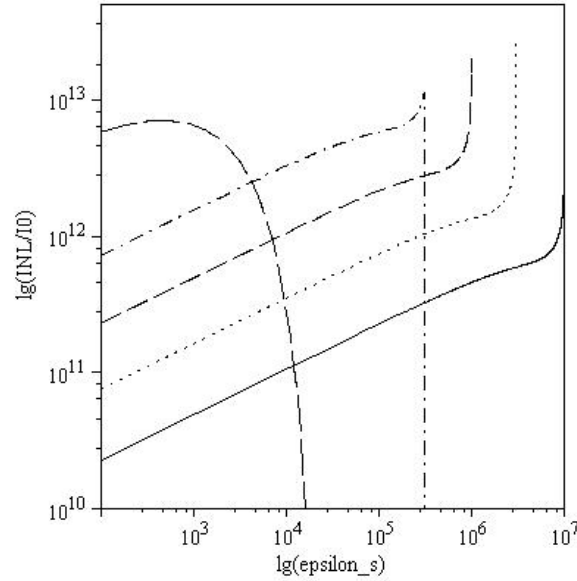


Figure 3.4: Normalised nonlinear synchrotron intensity I_{NL}/I_0 as a function of the energy ϵ_s at five different times $\tau = 0$ (solid curve), 10 (dotted curve), 10^2 (dashed curve), 10^3 (dash-dotted curve) and 10^5 (long-dashed curve).

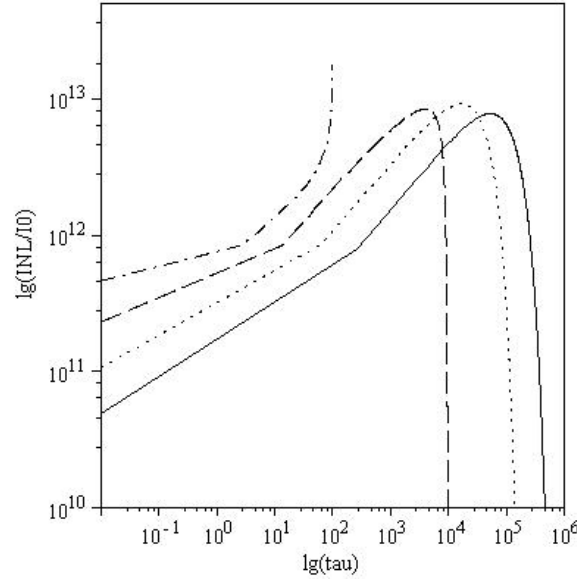


Figure 3.5: Normalised nonlinear synchrotron light curve I_{NL}/I_0 as a function of the time τ at four different energies $\epsilon_s = 10^3$ (solid curve), 10^4 (dotted curve), 10^5 (dashed curve) and 10^6 (dash-dotted curve).

Schlickeiser and Röken (2008), leading to the conclusion that the fluence behaviour for $\epsilon_s < \epsilon_{k,max}^{L,NL}$ is identical to the δ -distribution approximated Thomson regime fluence behaviour. Thus, we need only the optically thin synchrotron photon distributions (3.12) and (3.46) for the calculation of the synchrotron self-Compton fluence.

Linear electron cooling

With the linear synchrotron self-Compton intensity distribution (3.52) the synchrotron self-Compton fluence (3.22) reads for $\epsilon_s \geq \epsilon_{k,max}^L = 4\gamma_0^2\epsilon_0\omega_1^L$ and $t_0 = 0$

$$F_L(\epsilon_s) = F_0^L \epsilon_s \int_0^\infty (1 + \tau)^{8/3} a_1(\epsilon_s, \tau) f(\tau)^{2/3} H\left(\frac{\gamma_0}{\epsilon_s} - 1 - \tau\right) \cdot \left[\Gamma\left(-\frac{2}{3}, f(\tau)\bar{\Lambda}_L(\epsilon_s, \tau)\right) - f(\tau)\bar{\Lambda}_L(\epsilon_s, \tau) \Gamma\left(-\frac{5}{3}, f(\tau)\bar{\Lambda}_L(\epsilon_s, \tau)\right) \right] d\tau, \quad (3.55)$$

where $F_0^L = hRn_0/(4\pi D_0\gamma_0)$. We start with the computation of the fluence contribution for the first summand of the function $a_1(\epsilon_s, \tau)$. Substituting a new time-variable $z = 1 + \tau$ we obtain

$$F_L^{(1)}(\epsilon_s) = F_0^L \frac{\epsilon_s}{\epsilon_0^{2/3}} \int_1^{\gamma_0/\epsilon_s} z^4 \left[\Gamma\left(-\frac{2}{3}, \frac{\epsilon_s z^4}{4\gamma_0^2\epsilon_0(1 - \epsilon_s z/\gamma_0)}\right) - \frac{\epsilon_s z^4}{4\gamma_0^2\epsilon_0(1 - \epsilon_s z/\gamma_0)} \Gamma\left(-\frac{5}{3}, \frac{\epsilon_s z^4}{4\gamma_0^2\epsilon_0(1 - \epsilon_s z/\gamma_0)}\right) \right] dz. \quad (3.56)$$

Transforming $y = \epsilon_s z/\gamma_0$ and defining $\epsilon_f^L \equiv (\gamma_0^2/(4\epsilon_0))^{1/3}$, the integral yields

$$F_L^{(1)}(\epsilon_s) = F_0^L \frac{\gamma_0^5}{\epsilon_0^{2/3}\epsilon_s^4} \int_{\epsilon_s/\gamma_0}^1 y^4 \left[\Gamma\left(-\frac{2}{3}, \left(\frac{\epsilon_f^L}{\epsilon_s}\right)^3 \frac{y^4}{1-y}\right) - \left(\frac{\epsilon_f^L}{\epsilon_s}\right)^3 \frac{y^4}{1-y} \Gamma\left(-\frac{5}{3}, \left(\frac{\epsilon_f^L}{\epsilon_s}\right)^3 \frac{y^4}{1-y}\right) \right] dy. \quad (3.57)$$

For scattered photon energies $\epsilon_{k,max}^L \leq \epsilon_s < \epsilon_f^L$ the integrands contribution for $y \ll 1$ is dominating, so that (3.57) can be reduced to

$$F_L^{(1)}(\epsilon_s) = F_0^L \frac{\gamma_0^5}{\epsilon_0^{2/3} \epsilon_s^4} \int_{\epsilon_s/\gamma_0}^1 y^4 \left[\Gamma\left(-\frac{2}{3}, \left(\frac{\epsilon_f^L}{\epsilon_s}\right)^3 y^4\right) - \left(\frac{\epsilon_f^L}{\epsilon_s}\right)^3 y^4 \Gamma\left(-\frac{5}{3}, \left(\frac{\epsilon_f^L}{\epsilon_s}\right)^3 y^4\right) \right] dy. \quad (3.58)$$

Partial integration leads to the solution

$$\begin{aligned} F_L^{(1)}(\epsilon_s) = & F_0^L \frac{\gamma_0^5}{\epsilon_0^{2/3} \epsilon_s^4} \left(\frac{1}{5} \left[\Gamma\left(-\frac{2}{3}, \left(\frac{\epsilon_f^L}{\epsilon_s}\right)^3\right) - \left(\frac{\epsilon_s}{\gamma_0}\right)^5 \Gamma\left(-\frac{2}{3}, \frac{(\epsilon_f^L)^3 \epsilon_s}{\gamma_0^4}\right) \right. \right. \\ & + \left. \left. \left(\frac{\epsilon_s}{\epsilon_f^L}\right)^{15/4} \Gamma\left(\frac{7}{12}, \frac{(\epsilon_f^L)^3 \epsilon_s}{\gamma_0^4}, \left(\frac{\epsilon_f^L}{\epsilon_s}\right)^3\right) \right] - \frac{1}{9} \left[\left(\frac{\epsilon_f^L}{\epsilon_s}\right)^3 \Gamma\left(-\frac{5}{3}, \left(\frac{\epsilon_f^L}{\epsilon_s}\right)^3\right) \right. \right. \\ & \left. \left. - \frac{(\epsilon_f^L)^3 \epsilon_s^6}{\gamma_0^9} \Gamma\left(-\frac{5}{3}, \frac{(\epsilon_f^L)^3 \epsilon_s}{\gamma_0^4}\right) + \left(\frac{\epsilon_s}{\epsilon_f^L}\right)^{15/4} \Gamma\left(\frac{7}{12}, \frac{(\epsilon_f^L)^3 \epsilon_s}{\gamma_0^4}, \left(\frac{\epsilon_f^L}{\epsilon_s}\right)^3\right) \right] \right) \end{aligned} \quad (3.59)$$

consisting of incomplete and generalised incomplete Γ -functions multiplied by simple power functions. The argument $(\epsilon_f^L/\epsilon_s)^3$ is much larger than unity while the argument $(\epsilon_f^L)^3 \epsilon_s/\gamma_0^4$ is much smaller than unity. Hence, the fluence (3.59) can be approximated by

$$F_L^{(1)}(\epsilon_s) = \frac{4F_0^L \gamma_0^5}{45 \epsilon_0^{2/3} (\epsilon_f^L)^{15/4} \epsilon_s^{1/4}} \Gamma\left(\frac{7}{12}\right). \quad (3.60)$$

For large scattered photon energies $\epsilon_f^L < \epsilon_s \leq \gamma_0$, we split expression (3.57) for the fluence into two integrals, and after partial integration we obtain for the first integral

$$\begin{aligned} \int_{\epsilon_s/\gamma_0}^1 y^4 \Gamma\left(-\frac{2}{3}, \left(\frac{\epsilon_f^L}{\epsilon_s}\right)^3 \frac{y^4}{1-y}\right) dy = & -\frac{1}{5} \left(\frac{\epsilon_s}{\gamma_0}\right)^5 \Gamma\left(-\frac{2}{3}, \frac{(\epsilon_f^L)^3 \epsilon_s}{\gamma_0^4} \frac{1}{1-\frac{\epsilon_s}{\gamma_0}}\right) \\ & + \frac{1}{5} \left(\frac{\epsilon_s}{\epsilon_f^L}\right)^2 \int_{\epsilon_s/\gamma_0}^1 \left(\frac{1-y}{y}\right)^{5/3} \left(\frac{4y^3}{1-y} + \frac{y^4}{(1-y)^2}\right) \exp\left(-\left(\frac{\epsilon_f^L}{\epsilon_s}\right)^3 \frac{y^4}{1-y}\right) dy. \end{aligned} \quad (3.61)$$

Because all integrals in the high-energy scattered photon range are finally of the form of the integral on the right-hand-side of (3.61), we solve this in detail to demonstrate the used analytical methods. For this purpose the exponential function can be Taylor-expanded leading to

$$\int_{\epsilon_s/\gamma_0}^1 y^{4/3}(1-y)^{2/3} \exp\left(-\left(\frac{\epsilon_f^L}{\epsilon_s}\right)^3 \frac{y^4}{1-y}\right) dy = \sum_{n=0}^{\infty} \frac{1}{n!} \left(-\left[\frac{\epsilon_f^L}{\epsilon_s}\right]^3\right)^n \int_{\epsilon_s/\gamma_0}^1 \frac{y^{4n+4/3}}{(1-y)^{n-2/3}} dy. \quad (3.62)$$

The denominator of the integrand can be written as a generalised geometric series

$$\sum_{k=0}^{\infty} (a)_k \frac{x^k}{k!} = \frac{1}{(1-x)^a}, \quad (3.63)$$

where $(a)_k = a \cdot (a+1) \cdot (a+2) \cdots (a+k-1)$ is the Pochhammer symbol. Thus, the integral is simply solved by a sum of hypergeometric functions

$$\sum_{n=0}^{\infty} \sum_{k=0}^{\infty} \frac{(n-2/3)_k}{n!k!} \left(-\left[\frac{\epsilon_f^L}{\epsilon_s}\right]^3\right)^n \int_{\epsilon_s/\gamma_0}^1 y^{4n+k+4/3} dy = \quad (3.64)$$

$$\sum_{n=0}^{\infty} \frac{1}{n!} \left(-\left[\frac{\epsilon_f^L}{\epsilon_s}\right]^3\right)^n \frac{y^{4n+7/3}}{4n+7/3} {}_2F_1\left(4n+\frac{7}{3}, n-\frac{2}{3}; 4n+\frac{10}{3}; y\right) \Big|_{\epsilon_s/\gamma_0}^1.$$

The dominating contribution of the sum is of zeroth order, so that we obtain approximately

$$\frac{3}{7} y^{7/3} {}_2F_1\left(\frac{7}{3}, -\frac{2}{3}; \frac{10}{3}; y\right) \Big|_{\epsilon_s/\gamma_0}^1. \quad (3.65)$$

The whole solution of the integral (3.61) reads

$$\begin{aligned} & -\frac{1}{5} \left(\frac{\epsilon_s}{\gamma_0}\right)^5 \Gamma\left(-\frac{2}{3}, \frac{(\epsilon_f^L)^3 \epsilon_s}{\gamma_0^4} \frac{1}{1-\frac{\epsilon_s}{\gamma_0}}\right) + \frac{1}{5} \left(\frac{\epsilon_s}{\epsilon_f^L}\right)^2 \left(\frac{12}{7} y^{7/3} {}_2F_1\left(\frac{7}{3}, -\frac{2}{3}; \frac{10}{3}; y\right) \Big|_{\epsilon_s/\gamma_0}^1 + \frac{3}{10} \right. \\ & \cdot \left. y^{10/3} {}_2F_1\left(\frac{10}{3}, \frac{1}{3}; \frac{13}{3}; y\right) \Big|_{\epsilon_s/\gamma_0}^1\right) = -\frac{1}{5} \left(\frac{\epsilon_s}{\gamma_0}\right)^5 \Gamma\left(-\frac{2}{3}, \frac{(\epsilon_f^L)^3 \epsilon_s}{\gamma_0^4} \frac{1}{1-\frac{\epsilon_s}{\gamma_0}}\right) + \left(\frac{\epsilon_s}{\epsilon_f^L}\right)^2 \left(\frac{1}{14} \right. \\ & \cdot \left. \Gamma\left(\frac{2}{3}\right) \Gamma\left(\frac{10}{3}\right) - \frac{12}{35} \left(\frac{\epsilon_s}{\gamma_0}\right)^{7/3} {}_2F_1\left(\frac{7}{3}, -\frac{2}{3}; \frac{10}{3}; \frac{\epsilon_s}{\gamma_0}\right) - \frac{3}{50} \left(\frac{\epsilon_s}{\gamma_0}\right)^{10/3} {}_2F_1\left(\frac{10}{3}, \frac{1}{3}; \frac{13}{3}; \frac{\epsilon_s}{\gamma_0}\right)\right). \end{aligned} \quad (3.66)$$

The second integral of (3.57)

$$\begin{aligned}
 & - \left(\frac{\epsilon_f^L}{\epsilon_s} \right)^3 \int_{\epsilon_s/\gamma_0}^1 \frac{y^8}{1-y} \Gamma \left(-\frac{5}{3}, \left(\frac{\epsilon_f^L}{\epsilon_s} \right)^3 \frac{y^4}{1-y} \right) dy = \\
 & - \left(\frac{\epsilon_f^L}{\epsilon_s} \right)^3 \sum_{n=0}^{\infty} \int_{\epsilon_s/\gamma_0}^1 y^{n+8} \Gamma \left(-\frac{5}{3}, \left(\frac{\epsilon_f^L}{\epsilon_s} \right)^3 \frac{y^4}{1-y} \right) dy,
 \end{aligned} \tag{3.67}$$

yields the solution

$$\begin{aligned}
 & \left(\frac{\epsilon_f^L}{\epsilon_s} \right)^3 \Gamma \left(-\frac{5}{3}, \frac{(\epsilon_f^L)^3 \epsilon_s}{\gamma_0^4} \frac{1}{1-\frac{\epsilon_s}{\gamma_0}} \right) \sum_{n=0}^{\infty} \frac{(\epsilon_s/\gamma_0)^{n+9}}{n+9} - \left(\frac{\epsilon_s}{\epsilon_f^L} \right)^2 \sum_{n=0}^{\infty} \left(\frac{4y^{n+7/3}}{(n+7/3)(n+9)} \right. \\
 & \left. \cdot {}_2F_1 \left(n + \frac{7}{3}, -\frac{5}{3}; n + \frac{10}{3}; y \right) + \frac{y^{n+10/3}}{(n+10/3)(n+9)} {}_2F_1 \left(n + \frac{10}{3}, -\frac{2}{3}; n + \frac{13}{3}; y \right) \right) \Bigg|_{\epsilon_s/\gamma_0}^1.
 \end{aligned} \tag{3.68}$$

Defining *generalised dual hypergeometric functions*

$${}_p\mathcal{D}_q^l \left[\begin{matrix} c_1, \dots, c_k; d_1, \dots, d_l \\ a_1, \dots, a_p; b_1, \dots, b_q \end{matrix} \middle| x \right] := \sum_{n=0}^{\infty} \frac{(a_1)_n \dots (a_p)_n}{(b_1)_n \dots (b_q)_n} \frac{x^n}{n!} {}_kF_l(c_1, \dots, c_k; d_1, \dots, d_l; x), \tag{3.69}$$

the solution (3.68) can be written in a more compact form

$$\begin{aligned}
 & \frac{1}{9} \frac{(\epsilon_f^L)^3 \epsilon_s^6}{\gamma_0^9} \Gamma \left(-\frac{5}{3}, \frac{(\epsilon_f^L)^3 \epsilon_s}{\gamma_0^4} \frac{1}{1-\frac{\epsilon_s}{\gamma_0}} \right) {}_2F_1 \left(1, 9; 10; \frac{\epsilon_s}{\gamma_0} \right) - \left(\frac{\epsilon_s}{\epsilon_f^L} \right)^2 \left(\frac{4}{21} y^{7/3} \right. \\
 & \left. \cdot {}_3\mathcal{D}_2^1 \left[\begin{matrix} n + 7/3, -5/3; n + 10/3 \\ 1, 9, 7/3; 10, 10/3 \end{matrix} \middle| y \right] + \frac{1}{30} y^{10/3} {}_3\mathcal{D}_2^1 \left[\begin{matrix} n + 10/3, -2/3, n + 13/3 \\ 1, 9, 10/3; 10, 13/3 \end{matrix} \middle| y \right] \right) \Bigg|_{\epsilon_s/\gamma_0}^1.
 \end{aligned} \tag{3.70}$$

The whole first fluence contribution (3.57) then reads

$$\begin{aligned}
F_L^{(1)}(\epsilon_s) &= \frac{F_0^L \gamma_0^5}{\epsilon_0^{2/3} (\epsilon_f^L)^2 \epsilon_s^2} \left(\frac{1}{14} \Gamma\left(\frac{2}{3}\right) \Gamma\left(\frac{10}{3}\right) - \frac{12}{35} \left(\frac{\epsilon_s}{\gamma_0}\right)^{7/3} {}_2F_1\left(\frac{7}{3}, -\frac{2}{3}; \frac{10}{3}; \frac{\epsilon_s}{\gamma_0}\right) \right. \\
&\quad - \frac{3}{50} \left(\frac{\epsilon_s}{\gamma_0}\right)^{10/3} {}_2F_1\left(\frac{10}{3}, \frac{1}{3}; \frac{13}{3}; \frac{\epsilon_s}{\gamma_0}\right) - \frac{1}{5} \frac{(\epsilon_f^L)^2 \epsilon_s^3}{\gamma_0^5} \Gamma\left(-\frac{2}{3}, \frac{(\epsilon_f^L)^3 \epsilon_s}{\gamma_0^4} \frac{1}{1 - \frac{\epsilon_s}{\gamma_0}}\right) \\
&\quad + \frac{1}{9} \frac{(\epsilon_f^L)^5 \epsilon_s^4}{\gamma_0^9} \Gamma\left(-\frac{5}{3}, \frac{(\epsilon_f^L)^3 \epsilon_s}{\gamma_0^4} \frac{1}{1 - \frac{\epsilon_s}{\gamma_0}}\right) {}_2F_1\left(1, 9; 10; \frac{\epsilon_s}{\gamma_0}\right) \\
&\quad - \frac{4}{21} y^{7/32} {}_3D_2^1 \left[\begin{matrix} n + 7/3, -5/3; n + 10/3 \\ 1, 9, 7/3; 10, 10/3 \end{matrix} \middle| y \right]_{\epsilon_s/\gamma_0}^1 \\
&\quad \left. - \frac{1}{30} y^{10/3} {}_3D_2^1 \left[\begin{matrix} n + 10/3, -2/3, n + 13/3 \\ 1, 9, 10/3; 10, 13/3 \end{matrix} \middle| y \right]_{\epsilon_s/\gamma_0}^1 \right). \tag{3.71}
\end{aligned}$$

We obtain for the second term of $a_1(\epsilon_s, \tau)$ for $\epsilon_{k,max}^L \leq \epsilon_s < \epsilon_f^L$ a negligibly small fluence contribution

$$F_L^{(2)}(\epsilon_s) = \frac{2F_0^L \gamma_0^5 \epsilon_s^{5/4}}{77 \epsilon_0^{2/3} (\epsilon_f^L)^{21/4}} \Gamma\left(\frac{13}{12}\right) \ll F_L^{(1)}(\epsilon_s) \tag{3.72}$$

and for $\epsilon_f^L < \epsilon_s \leq \gamma_0$

$$\begin{aligned}
F_L^{(2)}(\epsilon_s) &= \frac{F_0^L \gamma_0^5}{\epsilon_0^{2/3} (\epsilon_f^L)^2 \epsilon_s^2} \left(-\frac{1}{14} \frac{(\epsilon_f^L)^2 \epsilon_s^5}{\gamma_0^7} \Gamma\left(-\frac{2}{3}, \frac{(\epsilon_f^L)^3 \epsilon_s}{\gamma_0^4} \frac{1}{1 - \frac{\epsilon_s}{\gamma_0}}\right) {}_2F_1\left(1, 7; 8; \frac{\epsilon_s}{\gamma_0}\right) \right. \\
&\quad \left. + \frac{1}{22} \frac{(\epsilon_f^L)^5 \epsilon_s^6}{\gamma_0^{11}} \Gamma\left(-\frac{5}{3}, \frac{(\epsilon_f^L)^3 \epsilon_s}{\gamma_0^4} \frac{1}{1 - \frac{\epsilon_s}{\gamma_0}}\right) {}_2F_1\left(2, 11; 12; \frac{\epsilon_s}{\gamma_0}\right) \right)
\end{aligned}$$

$$\begin{aligned}
 & + \frac{6}{91} y^{13/3} {}_3\mathcal{D}_2^1 \left[\begin{matrix} n + 13/3, -2/3; n + 16/3 \\ 1, 7, 13/3; 8, 16/3 \end{matrix} \middle| y \right] \Big|_{\epsilon_s/\gamma_0}^1 \\
 & + \frac{3}{224} y^{16/3} {}_3\mathcal{D}_2^1 \left[\begin{matrix} n + 16/3, 1/3, n + 19/3 \\ 1, 7, 16/3; 8, 19/3 \end{matrix} \middle| y \right] \Big|_{\epsilon_s/\gamma_0}^1 \\
 & - \frac{6}{143} y^{13/3} {}_3\mathcal{D}_2^1 \left[\begin{matrix} n + 13/3, -5/3; n + 16/3 \\ 2, 11, 13/3; 12, 16/3 \end{matrix} \middle| y \right] \Big|_{\epsilon_s/\gamma_0}^1 \\
 & - \frac{3}{352} y^{16/3} {}_3\mathcal{D}_2^1 \left[\begin{matrix} n + 16/3, -2/3, n + 19/3 \\ 2, 11, 16/3; 12, 19/3 \end{matrix} \middle| y \right] \Big|_{\epsilon_s/\gamma_0}^1 \Bigg),
 \end{aligned} \tag{3.73}$$

where the total fluence is finally $F_L(\epsilon_s) = F_L^{(1)}(\epsilon_s) + F_L^{(2)}(\epsilon_s)$.

Nonlinear electron cooling

Using the nonlinear synchrotron self-Compton intensity (3.54) the nonlinear synchrotron self-Compton fluence reads for $\epsilon_s \geq \epsilon_{k,max}^{NL} = 4\gamma_0^2 \epsilon_0 \omega_1^{NL}$

$$\begin{aligned}
 F_{NL}(\epsilon_s) = F_0^{NL} \epsilon_s \int_0^\infty (1 + \tau)^{7/6} b_1(\epsilon_s, \tau) g(\tau)^{2/3} H\left(\frac{\gamma_0^2}{\epsilon_s^2} - 1 - \tau\right) \\
 \cdot \left[\Gamma\left(-\frac{2}{3}, g(\tau) \bar{\Lambda}_{NL}(\epsilon_s, \tau)\right) - g(\tau) \bar{\Lambda}_{NL}(\epsilon_s, \tau) \Gamma\left(-\frac{5}{3}, g(\tau) \bar{\Lambda}_{NL}(\epsilon_s, \tau)\right) \right] d\tau,
 \end{aligned} \tag{3.74}$$

where $F_0^{NL} = hRn_0/(8\pi A_0 q_0 \gamma_0^2)$. Defining $\epsilon_f^{NL} = \gamma_0^{5/7}/(4\epsilon_0)^{2/7}$ and using the same methods as for the linear case we obtain for $\epsilon_{k,max}^{NL} \leq \epsilon_s < \epsilon_f^{NL}$

$$F_{NL}^{(1)}(\epsilon_s) = \frac{F_0^{NL} \gamma_0^6}{7\epsilon_0^{2/3} (\epsilon_f^{NL})^{14/3} \epsilon_s^{1/3}} \Gamma\left(\frac{2}{3}\right) \tag{3.75}$$

and

$$F_{NL}^{(2)}(\epsilon_s) = \frac{9F_0^{NL} \gamma_0^6 \epsilon_s^{11/9}}{200\epsilon_0^{2/3} (\epsilon_f^{NL})^{56/9}} \Gamma\left(\frac{10}{9}\right) \ll F_{NL}^{(1)}(\epsilon_s) \tag{3.76}$$

as well as for $\epsilon_f^{NL} < \epsilon_s \leq \gamma_0$

$$\begin{aligned}
 F_{NL}^{(1)}(\epsilon_s) &= \frac{F_0^{NL} \gamma_0^6}{\epsilon_0^{2/3} (\epsilon_f^{NL})^{7/3} \epsilon_s^{8/3}} \left(\frac{81}{220} - \frac{1}{2} \left(\frac{\epsilon_s}{\gamma_0} \right)^3 {}_2F_1 \left(3, -\frac{2}{3}; 4; \frac{\epsilon_s}{\gamma_0} \right) - \frac{1}{12} \left(\frac{\epsilon_s}{\gamma_0} \right)^4 \right. \\
 &\cdot {}_2F_1 \left(4, \frac{1}{3}; 5; \frac{\epsilon_s}{\gamma_0} \right) - \frac{1}{3} \frac{(\epsilon_f^{NL})^{7/3} \epsilon_s^{11/3}}{\gamma_0^6} \Gamma \left(-\frac{2}{3}, \frac{(\epsilon_f^{NL})^{7/2} \epsilon_s}{\gamma_0^{9/2}} \frac{1}{1 - \frac{\epsilon_s}{\gamma_0}} \right) \\
 &+ \frac{4}{21} \frac{(\epsilon_f^{NL})^{35/6} \epsilon_s^{14/3}}{\gamma_0^{21/2}} \Gamma \left(-\frac{5}{3}, \frac{(\epsilon_f^{NL})^{7/2} \epsilon_s}{\gamma_0^{9/2}} \frac{1}{1 - \frac{\epsilon_s}{\gamma_0}} \right) {}_2F_1 \left(1, \frac{21}{2}; \frac{23}{2}; \frac{\epsilon_s}{\gamma_0} \right) \\
 &\left. - \frac{2}{7} y^3 {}_3\mathcal{D}_2^1 \left[\begin{matrix} n+3, -5/3; n+4 \\ 1, 3, 21/2; 4, 23/2 \end{matrix} \middle| y \right] \Big|_{\epsilon_s/\gamma_0}^1 - \frac{1}{21} y^4 {}_3\mathcal{D}_2^1 \left[\begin{matrix} n+4, -2/3, n+5 \\ 1, 4, 21/2; 5, 23/2 \end{matrix} \middle| y \right] \Big|_{\epsilon_s/\gamma_0}^1 \right) \quad (3.77)
 \end{aligned}$$

and

$$\begin{aligned}
 F_{NL}^{(2)}(\epsilon_s) &= \frac{F_0^{NL} \gamma_0^6}{\epsilon_0^{2/3} (\epsilon_f^{NL})^{7/3} \epsilon_s^{8/3}} \left(-\frac{1}{8} \frac{(\epsilon_f^{NL})^{7/3} \epsilon_s^{17/3}}{\gamma_0^8} \Gamma \left(-\frac{2}{3}, \frac{(\epsilon_f^{NL})^{7/2} \epsilon_s}{\gamma_0^{9/2}} \frac{1}{1 - \frac{\epsilon_s}{\gamma_0}} \right) \right. \\
 &{}_2F_1 \left(1, 8; 9; \frac{\epsilon_s}{\gamma_0} \right) + \frac{2}{25} \frac{(\epsilon_f^{NL})^{35/6} \epsilon_s^{20/3}}{\gamma_0^{25/2}} \Gamma \left(-\frac{5}{3}, \frac{(\epsilon_f^{NL})^{7/2} \epsilon_s}{\gamma_0^{9/2}} \frac{1}{1 - \frac{\epsilon_s}{\gamma_0}} \right) {}_2F_1 \left(2, \frac{25}{2}; \frac{27}{2}; \frac{\epsilon_s}{\gamma_0} \right) \\
 &+ \frac{9}{80} y^5 {}_3\mathcal{D}_2^1 \left[\begin{matrix} n+5, -2/3; n+6 \\ 1, 5, 8; 6, 9 \end{matrix} \middle| y \right] \Big|_{\epsilon_s/\gamma_0}^1 + \frac{1}{48} y^6 {}_3\mathcal{D}_2^1 \left[\begin{matrix} n+6, 1/3, n+7 \\ 1, 6, 8; 7, 9 \end{matrix} \middle| y \right] \Big|_{\epsilon_s/\gamma_0}^1 \\
 &\left. - \frac{9}{125} y^5 {}_3\mathcal{D}_2^1 \left[\begin{matrix} n+5, -5/3; n+6 \\ 2, 5, 25/2; 6, 27/2 \end{matrix} \middle| y \right] \Big|_{\epsilon_s/\gamma_0}^1 - \frac{1}{75} y^6 {}_3\mathcal{D}_2^1 \left[\begin{matrix} n+6, -2/3, n+7 \\ 2, 6, 25/2; 7, 27/2 \end{matrix} \middle| y \right] \Big|_{\epsilon_s/\gamma_0}^1 \right). \quad (3.78)
 \end{aligned}$$

In Figures 3.6 and 3.7, we show the linear, (3.71) and (3.73), and the nonlinear fluence distribution (3.77) and (3.78) (solid curves) in comparison to the δ -distribution

approximated Thomson regime restricted fluence distributions (dashed curves)

$$F_L^\delta(\epsilon_s) = \frac{12}{7} F_0^{L,\delta} \frac{\epsilon_f}{\epsilon_s^2} \left[1 - \left(\frac{\epsilon_s}{\gamma_0} \right)^{7/3} \right] \quad (3.79)$$

and

$$F_{NL}^\delta(\epsilon_s) = \frac{2}{3} F_0^{NL,\delta} \frac{\epsilon_f^{7/6}}{\epsilon_s^{8/3}} \left[1 - \left(\frac{\epsilon_s}{\gamma_0} \right)^3 \right]. \quad (3.80)$$

Despite the different functional form of the full Klein-Nishina fluence distributions and the approximated fluence distributions in the high-energy regime in both electron synchrotron cooling cases the plots look nearly identical (except for negligible small variations in the magnitude) due to the averaged cancellation of the *significant* additional contributions of the full Klein-Nishina fluence distribution among each other.

3.3 Discussion

Schlickeiser and Lerche (2007) developed a nonlinear model for the synchrotron radiation cooling of ultra-relativistic particles in powerful non-thermal radiation sources assuming a partition condition between the energy densities of the magnetic field and the relativistic electrons. Here, we used this model in order to calculate the synchrotron self-Compton process in flaring TeV blazars and compared it to the results obtained with the standard linear synchrotron cooling model.

For simplicity, we chose the case of instantaneously injected monoenergetic relativistic electrons as an illustrative example, although other injection scenarios like the instantaneous injection of power-law distributed electrons (Schlickeiser and Lerche, 2008) are also possible. After the *nonlinear* electron synchrotron radiation cooling the created synchrotron photons with non-relativistic energies are multiple Thomson scattered off the cooled electrons in the source (synchrotron self-Compton process).

We calculated the optically thin and thick synchrotron radiation intensities as well as the synchrotron photon density distributions in the emission knot as functions of frequency and time. These synchrotron photons serve as target photons in the synchrotron

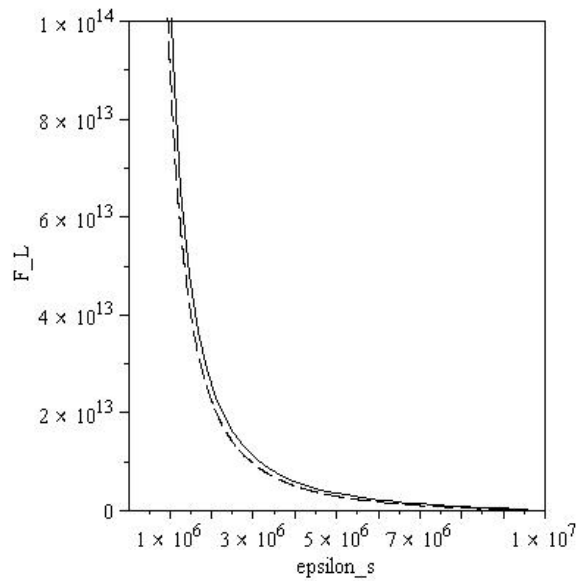


Figure 3.6: Normalised linear fluence distributions for the full Klein-Nishina cross section (solid curve) and for the δ -distribution approximated cross section (dashed curve) for $\epsilon_f^L < \epsilon_s \leq \gamma_0$ with $\gamma_0 = 10^7$.

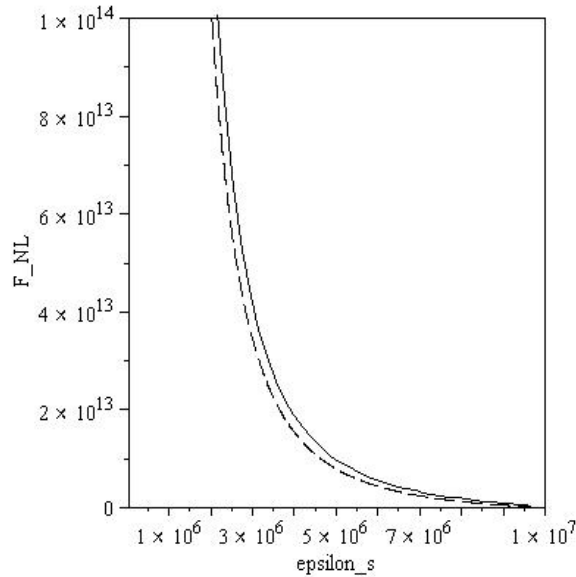


Figure 3.7: Normalised nonlinear fluence distributions for the full Klein-Nishina cross section (solid curve) and for the δ -distribution approximated cross section (dashed curve) for $\epsilon_f^{NL} < \epsilon_s \leq \gamma_0$ with $\gamma_0 = 10^7$.

self-Compton process. Using the Thomson approximation of the inverse Compton cross section we determined the synchrotron self-Compton intensity and fluence for a *non-linear* electron cooling. It is shown that the optically thick synchrotron radiation component provides only a negligible contribution to the synchrotron self-Compton quantities at all frequencies and times as in the linear cooling case.

In the following, we compared the linear to the nonlinear fluence distribution fitting both to the observed TeV fluence spectrum of PKS 2155-304 on MJD 53944 and performed a statistical quality-of-fit test (AIC test). For this particular data record we found the linear model to be more appropriate than the nonlinear. To transform this indication into a solid conclusion we have, thus, to perform tests on more statistical ensembles.

Nonetheless, the excellent agreement of both, linear and nonlinear synchrotron self-Compton fluence spectra with the observation of the gamma-ray flare of PKS 2155-304 support the injection scenario of *monoenergetic* electrons by the relativistic pick-up process.

To generalise the δ -distribution approximation results we discussed the linear and nonlinear synchrotron self-Compton scattering processes of flaring TeV blazar sources utilising the *full Klein-Nishina cross section* for the computation of the inverse Compton scattering rate.

We obtained only fluence distributions with *additional non-vanishing* contributions in the high-energy regime $\epsilon_f^{L,NL} < \epsilon_s \leq \gamma_0$ of the scattered photons, e.g. generalised incomplete Γ -functions or the new generalised dual hypergeometric functions. Surprisingly, for the special class of electron and synchrotron photon distributions used in this work these contributions cancel each other out in average. Hence, it can be justified to model the photon spectra by applying the δ -distribution approximation for the calculation of the differential inverse Compton scattering rate for electron and synchrotron densities of the form (3.45), (3.46) as well as (2.7) and (3.12).

4 Summary and Conclusions

In this thesis, we investigated analytically the double-peak profile of the emission of powerful cosmic non-thermal radiation sources with dominant magnetic field self-generation like TeV blazars. Therefore, we used the well established linear model and for the first time the recently introduced nonlinear electron synchrotron cooling model developed by Schlickeiser and Lerche (2007).

We assumed a flare to occur in the emission knot, propagating in the jet of an active galactic nucleus, at the time $t = t_0$ due to the uniform instantaneous injection of monoenergetic ultra-relativistic electrons via the relativistic pick-up process. At later times the electrons are subjected to a linear or nonlinear synchrotron radiation cooling. In the first, linear scenario the magnetic field is constant, while in the second the magnetic field is time-dependent and adjusts its strength to the energy density of the injected electrons. These synchrotron photons produced in this way most probably cause the low-energy peak in the blazar spectra. Afterwards, they are multiple Thomson scattered off their generating electrons. This is the so-called synchrotron self-Compton process, which we presumed to be responsible for the high-energy peak.

For our investigation of the low-energy peak, we succeeded in working out the differences between *single* and *multiple* instantaneous injections of monoenergetic relativistic electrons by solving the linear and nonlinear kinetic equations for the intrinsic temporal evolution of relativistic electrons and by calculating the associated radiation formulas. This is of great interest, because it is very likely that electron injections into the plasmoids occur repeatedly, so that this would explain substructures in high-resolution measurements of the synchrotron peak. Substructures in a system with nonlinear electron cooling would be completely different to those of a system with linear electron cooling, since the nonlinear model magnetic field depends on time and on the number of injections (see for example Figures 2.6 and 2.7), whereas the linear model magnetic field is constant.

For our study of the high-energy peak we computed the optically thin and thick synchrotron radiation intensities and photon density distributions of one instantaneous injection of monoenergetic electrons in the emission knot as functions of frequency and time analytically, followed by the synchrotron self-Compton intensity and fluence using the δ -distribution approximation in the Thomson limit of the inverse Compton cross section. For all times and frequencies the optically thin part of the synchrotron radiation process is demonstrated to provide the dominating contribution to the synchrotron self-Compton quantities, while the optically thick part is always negligible.

In the following, we compared the linear to the nonlinear synchrotron radiation cooling models using one of the data records of the time-averaged spectra of PKS 2155-304 on MJD 53944 favouring a *linear* cooling of the injected monoenergetic electrons. *The surprisingly good agreement of both, the linear and nonlinear cooling models with the data strongly supports the theory of the relativistic pick-up process of simple monoenergetic electrons operating in this source.*

Finally, to obtain most general results, we applied the full Klein-Nishina cross section to the inverse Compton scattering rate. We found, for the first time, that functional differences in comparison to the δ -distribution approximation occurred only in the high-energy regime of the synchrotron self-Compton intensity and fluence distributions. These unanticipatedly compensate each other in average, so that the less intricate δ -distribution approximation appears to be appropriate for future calculations with the special class of density distributions utilised in this work.

Prospective topics regarding the subject discussed here can be addressed. Numerical simulations of the synchrotron intensity and fluence distributions for more than four injections are required, as well as an analytical description of the intrinsic *optically thick* synchrotron radiation formulas for multiple injections in the nonlinear electron synchrotron cooling case for the claim of completeness. Moreover, to obtain *definite* results in favour of the linear cooling model, further quality-of-fit tests on additional data records have to be performed.

In conclusion, we notice that our investigation of emission processes in powerful cosmic non-thermal radiation sources with dominant magnetic field self-generation indicates that these arise most likely from the instantaneous injection of *monoenergetic* electrons via the relativistic pick-up process (see Figure 3.1). Also, conceivable substructures in the synchrotron emission peak can be explained by the scenario of *multiple* monoenergetic injections.

A Single electron differential scattering rate

To solve the ϵ' -integration in the single electron differential scattering rate

$$\begin{aligned} \frac{d^2 N}{dt d\epsilon_s} &\simeq \frac{\pi r_0^2 c}{2\gamma^2 \epsilon_s} \int_0^\infty \frac{n(\epsilon)}{\epsilon^2} \int_0^\infty \int_{-1}^1 \delta(\epsilon'_s - \epsilon'_0) H\left(\epsilon' - \frac{\epsilon}{2\gamma}\right) H(2\gamma\epsilon - \epsilon') \\ &\cdot \frac{\epsilon_s^3}{\epsilon'} \left(\frac{\epsilon'}{\epsilon'_s} + \frac{\epsilon'_s}{\epsilon'} - \sin^2 \chi' \right) d \cos \chi' d\epsilon' d\epsilon \end{aligned} \quad (\text{A.1})$$

we have to transform the Dirac distribution

$$\delta(\epsilon'_s - \epsilon'_0) = \left(1 - \epsilon'_s(1 - \cos \chi')\right)^{-2} \cdot \delta\left(\epsilon' - \frac{\epsilon'_s}{1 - \epsilon'_s(1 - \cos \chi')}\right). \quad (\text{A.2})$$

We then obtain

$$\begin{aligned} \frac{d^2 N}{dt d\epsilon_s} &\simeq \frac{\pi r_0^2 c}{2\gamma^2 \epsilon_s} \int_0^\infty \frac{n(\epsilon)}{\epsilon^2} \int_{-1}^1 \frac{\epsilon_s'^2}{1 - \epsilon'_s(1 - \cos \chi')} \left(\left[1 - \epsilon'_s(1 - \cos \chi')\right]^{-1} \right. \\ &\left. - \epsilon'_s(1 - \cos \chi') + \cos^2 \chi' \right) H\left(\frac{\epsilon'_s}{1 - \epsilon'_s(1 - \cos \chi')} - \frac{\epsilon}{2\gamma}\right) \\ &\cdot H\left(2\gamma\epsilon - \frac{\epsilon'_s}{1 - \epsilon'_s(1 - \cos \chi')}\right) d \cos \chi' d\epsilon. \end{aligned} \quad (\text{A.3})$$

The scattered photon energy in the electron rest frame with respect to the scattered photon energy in the comoving frame $\epsilon'_s = \epsilon_s/(\gamma(1 - \beta \cos \chi'))$ yields, using the head-on approximation, $\epsilon_s = \gamma\epsilon'_s(1 + \beta \cos \psi'_s)$. Substituting $\eta = 1 - \beta \cos \chi'$ we obtain

$$\begin{aligned} \frac{d^2 N}{dt d\epsilon_s} &\simeq \frac{\pi r_0^2 c \epsilon_s}{2\gamma^4} \left[1 - \frac{\epsilon_s}{\gamma}\right]^{-1} \int_0^\infty \frac{n(\epsilon)}{\epsilon^2} \int_{1/2\gamma^2}^2 \frac{1}{\eta^2} \left(\eta^2 + 2(1-\eta) + \frac{\epsilon_s^2}{\gamma^2(1-\epsilon_s/\gamma)} \right) \\ &\cdot H\left(\frac{2\epsilon_s}{\epsilon(1-\epsilon_s/\gamma)} - \eta\right) H\left(\eta - \frac{\epsilon_s}{2\gamma^2\epsilon(1-\epsilon_s/\gamma)}\right) d\eta d\epsilon, \end{aligned} \quad (\text{A.4})$$

where $\beta \approx 1$ leading to $1-\beta = 1/(\gamma^2(1+\beta)) \approx 1/(2\gamma^2)$. With $c_1 \equiv 2+\epsilon_s^2/(\gamma^2(1-\epsilon_s/\gamma))$, $c_2 \equiv \epsilon_s/(2\gamma^2\epsilon(1-\epsilon_s/\gamma))$ and $c_3 \equiv 4\gamma^2 c_2$ the η -integration can be solved by

$$\begin{aligned} &\int_{1/2\gamma^2}^2 \left(1 - \frac{2}{\eta} + \frac{c_1}{\eta^2}\right) H(\eta - c_2) H(\eta - c_3) d\eta = \left[H(\eta - c_2) H(c_3 - \eta) \right. \\ &\cdot \left. \left(\eta - 2 \ln(\eta) - \frac{c_1}{\eta} \right) - H(c_3 - c_2) H(\eta - c_2) \left(c_2 - 2 \ln(c_2) - \frac{c_1}{c_2} \right) \right. \\ &\left. + H(c_3 - c_2) H(\eta - c_3) \left(c_3 - 2 \ln(c_3) - \frac{c_1}{c_3} \right) \right] \Big|_{1/2\gamma^2}^2. \end{aligned} \quad (\text{A.5})$$

After inserting the boundaries of integration and simple algebra we obtain

$$\begin{aligned} &H\left(\underbrace{\epsilon - \frac{\epsilon_s}{4\gamma^2(1-\frac{\epsilon_s}{\gamma})}}_{=: \epsilon\Lambda(\epsilon, \epsilon_s)}\right) H(\epsilon_s - \epsilon) \\ &\cdot \left[\overbrace{1 + 2 \ln\left(\frac{\epsilon_s}{4\gamma^2\epsilon(1-\frac{\epsilon_s}{\gamma})}\right) - \frac{\epsilon_s^2 + \epsilon_s/\epsilon}{2\gamma^2(1-\frac{\epsilon_s}{\gamma})} + 2\epsilon\epsilon_s + \frac{4\gamma^2\epsilon(1-\frac{\epsilon_s}{\gamma})}{\epsilon_s}}^{\text{high-energy contribution}} \right] \\ &- H(\epsilon - \epsilon_s) H(4\gamma^2\epsilon_s - \epsilon) \\ &\cdot \left[\overbrace{\underbrace{\frac{1}{2\gamma^2}}_{\rightarrow 0} - 4\gamma^2 + 2 \ln\left(\underbrace{\frac{4\gamma^2\epsilon_s}{\epsilon(1-\frac{\epsilon_s}{\gamma})}}_{\rightarrow 4\gamma^2\epsilon_s/\epsilon}\right) - \underbrace{\frac{2\epsilon_s^2}{1-\frac{\epsilon_s}{\gamma}}}_{\rightarrow 2\epsilon_s^2 \ll 4\gamma^2} - \underbrace{\frac{2\epsilon_s}{\epsilon(1-\frac{\epsilon_s}{\gamma})}}_{\rightarrow 2\epsilon_s/\epsilon} + \underbrace{\frac{\epsilon\epsilon_s}{2\gamma^2}}_{\rightarrow 0} + \underbrace{\frac{\epsilon}{\epsilon_s}\left(1-\frac{\epsilon_s}{\gamma}\right)}_{\rightarrow \epsilon/\epsilon_s}}^{\text{low-energy contribution}} \right] \end{aligned}$$

$$\begin{aligned}
&\approx H(1 - \Lambda(\epsilon, \epsilon_s))H(\epsilon_s - \epsilon) \left[(1 - \Lambda(\epsilon, \epsilon_s)) \left(\frac{1}{\Lambda(\epsilon, \epsilon_s)} + 2[1 + \epsilon_s \epsilon] \right) + 2 \ln(\Lambda(\epsilon, \epsilon_s)) \right] \\
&+ H(\epsilon - \epsilon_s)H(4\gamma^2 \epsilon_s - \epsilon) \left[\underbrace{4\gamma^2 + 2 \ln \left(\frac{\epsilon}{4\gamma^2 \epsilon_s} \right) + \frac{2\epsilon_s}{\epsilon} - \frac{\epsilon}{\epsilon_s}}_{\rightarrow 4\gamma^2} \right].
\end{aligned} \tag{A.6}$$

Thus, (A.4) reads

$$\begin{aligned}
\frac{d^2 N}{dt d\epsilon_s} &\simeq \frac{\pi r_0^2 c}{2\gamma^4} \int_0^\infty \frac{n(\epsilon)}{\epsilon} \left(4\gamma^2 H(1 - \Lambda(\epsilon, \epsilon_s))H(\epsilon_s - \epsilon) \right. \\
&\cdot \left. \left[(1 - \Lambda(\epsilon, \epsilon_s)) \left(1 + 2\Lambda(\epsilon, \epsilon_s)[1 + \epsilon_s \epsilon] \right) + 2\Lambda(\epsilon, \epsilon_s) \ln(\Lambda(\epsilon, \epsilon_s)) \right] \right. \\
&\left. + H(\epsilon - \epsilon_s)H(4\gamma^2 \epsilon_s - \epsilon) \left[4\gamma^2 \frac{\epsilon_s}{\epsilon} - 1 \right] \right) d\epsilon.
\end{aligned} \tag{A.7}$$

B Solution of the electron kinetic equation with two injections for linear cooling

Inserting the energy loss rate $|\dot{\gamma}| = D_0\gamma^2$ with the constant rate D_0 into the kinetic equation (2.2) yields

$$\frac{\partial n(\gamma, t)}{\partial t} - D_0 \frac{\partial}{\partial \gamma} (\gamma^2 n(\gamma, t)) = q_0 \delta(\gamma - \gamma_0) \delta(t - t_0) + q_1 \delta(\gamma - \gamma_1) \delta(t - t_1). \quad (\text{B.1})$$

With the time variable $\tau = D_0 t$ and the function $R = \gamma^2 n$ the kinetic equation reads

$$\frac{\partial R(\gamma, \tau)}{\partial \tau} - \gamma^2 \frac{\partial R(\gamma, \tau)}{\partial \gamma} = q_0 \gamma^2 \delta(\gamma - \gamma_0) \delta(\tau - \tau_0) + q_1 \gamma^2 \delta(\gamma - \gamma_1) \delta(\tau - \tau_1). \quad (\text{B.2})$$

Substitution of $x = \gamma^{-1}$ finally yields

$$\frac{\partial R(x, \tau)}{\partial \tau} + \frac{\partial R(x, \tau)}{\partial x} = q_0 \delta(x - x_0) \delta(\tau - \tau_0) + q_1 \delta(x - x_1) \delta(\tau - \tau_1). \quad (\text{B.3})$$

This equation is immediately solved by Laplace transformations with respect to τ and x . Multiplying (B.3) with e^{-sx} and integrating over the positive x -space we obtain using $F(s, \tau) = \int_0^\infty e^{-sx} R(x, \tau) dx$

$$\underbrace{\int_0^\infty e^{-sx} \frac{\partial R(x, \tau)}{\partial \tau} dx}_{=\frac{\partial F(s, \tau)}{\partial \tau}} + \underbrace{\int_0^\infty e^{-sx} \frac{\partial R(x, \tau)}{\partial x} dx}_{=e^{-sx} R(x, \tau) \Big|_0^\infty + sF(s, \tau)} = q_0 \delta(\tau - \tau_0) \int_0^\infty e^{-sx} \delta(x - x_0) dx + q_1 \delta(\tau - \tau_1) \int_0^\infty e^{-sx} \delta(x - x_1) dx. \quad (\text{B.4})$$

Under consideration of the boundary condition $R(0, \tau) = 0$ we find

$$\frac{\partial F(s, \tau)}{\partial \tau} + sF(s, \tau) = q_0 \delta(\tau - \tau_0) e^{-s x_0} + q_1 \delta(\tau - \tau_1) e^{-s x_1}. \quad (\text{B.5})$$

The second Laplace transformation $Q(s, w) = \int_0^\infty e^{-w\tau} F(s, \tau) d\tau$ with the boundary condition $F(s, 0) = 0$ results, after a simple equivalence transformation, in

$$Q(s, w) = \frac{q_0 e^{-s x_0} e^{-w \tau_0} + q_1 e^{-s x_1} e^{-w \tau_1}}{s + w}. \quad (\text{B.6})$$

Thus, the original function $R(x, \tau)$ is

$$R(x, \tau) = q_0 H(x - x_0) \delta(x - x_0 - \tau + \tau_0) + q_1 H(x - x_1) \delta(x - x_1 - \tau + \tau_1). \quad (\text{B.7})$$

The linear electron density distribution can be computed to

$$n(\gamma, \tau) = \gamma^{-2} R(\gamma, \tau) = q_0 H(\gamma_0 - \gamma) \delta(\gamma - \gamma_L^{(0)}) + q_1 H(\gamma_1 - \gamma) \delta(\gamma - \gamma_L^{(1)}) \quad (\text{B.8})$$

with $\gamma_L^{(k)} = \gamma_k / (1 + D_0 \gamma_k (t - t_k))$. The solution for the kinetic equation for $m + 1$ injections

$$\frac{\partial n(\gamma, t)}{\partial t} - D_0 \frac{\partial}{\partial \gamma} (\gamma^2 n(\gamma, t)) = \sum_{k=0}^m q_k \delta(\gamma - \gamma_k) \delta(t - t_k) \quad (\text{B.9})$$

can be easily found generalising the result (B.8)

$$n(\gamma, \tau) = \sum_{k=0}^m q_k H(\gamma_k - \gamma) \delta(\gamma - \gamma_L^{(k)}). \quad (\text{B.10})$$

C Solution of the electron kinetic equation with two injections for nonlinear cooling

Under the partition condition $e_B = U_B(t)/U_e(t)$ the evolution of the population of relativistic electrons is described by the kinetic equation

$$\begin{aligned} \frac{\partial n(\gamma, t)}{\partial t} - A_0 \left(\int_0^\infty \gamma n(\gamma, t) d\gamma \right) \frac{\partial}{\partial \gamma} (\gamma^2 n(\gamma, t)) &= q_0 \delta(\gamma - \gamma_0) \delta(t - t_0) \\ &+ q_1 \delta(\gamma - \gamma_1) \delta(t - t_1). \end{aligned} \quad (\text{C.1})$$

The substitution of $\tau = A_0 t$ and $S = \gamma^2 n$ results in the equation

$$\begin{aligned} \frac{\partial S(\gamma, \tau)}{\partial \tau} - \gamma^2 \left(\int_0^\infty \frac{S(\gamma, \tau)}{\gamma} d\gamma \right) \frac{\partial S(\gamma, \tau)}{\partial \gamma} &= q_0 \gamma^2 \delta(\gamma - \gamma_0) \delta(\tau - \tau_0) \\ &+ q_1 \gamma^2 \delta(\gamma - \gamma_1) \delta(\tau - \tau_1). \end{aligned} \quad (\text{C.2})$$

Once again we use the variable $x = \gamma^{-1}$. Hence, the kinetic equation readily yields

$$\begin{aligned} \frac{\partial S(x, \tau)}{\partial \tau} + \left(\int_0^\infty \frac{S(x, \tau)}{x} dx \right) \frac{\partial S(x, \tau)}{\partial x} &= q_0 \delta(x - x_0) \delta(\tau - \tau_0) \\ &+ q_1 \delta(x - x_1) \delta(\tau - \tau_1). \end{aligned} \quad (\text{C.3})$$

Defining a function $T(\tau)$ through the integro-differential equation

$$\int_0^\infty \frac{S(\gamma, \tau)}{\gamma} d\gamma = U(\tau) = \frac{dT(\tau)}{d\tau} \quad (\text{C.4})$$

we obtain the form

$$\frac{\partial S(x, T)}{\partial T} + \frac{\partial S(x, T)}{\partial x} = q_0 \delta(x - x_0) \frac{\delta(\tau - \tau_0)}{U(\tau)} + q_1 \delta(x - x_1) \frac{\delta(\tau - \tau_1)}{U(\tau)}. \quad (\text{C.5})$$

Laplace transformations regarding x and T (see Appendix B), requiring the boundary conditions $S(x, 0) = 0$ and $\int_0^\infty e^{-wT} S(0, T) dT = 0$, constitute the solution

$$\begin{aligned} S(x, T) = & q_0 \delta(x - x_0 - T(\tau) + T(\tau_0)) H(T - T(\tau_0)) \\ & + q_1 \delta(x - x_1 - T(\tau) + T(\tau_1)) H(T - T(\tau_1)). \end{aligned} \quad (\text{C.6})$$

Solving the nonlinear kinetic equation for $m + 1$ injections

$$\frac{\partial n(\gamma, t)}{\partial t} - A_0 \left(\int_0^\infty \gamma n(\gamma, t) d\gamma \right) \frac{\partial}{\partial \gamma} (\gamma^2 n(\gamma, t)) = \sum_{k=0}^m q_k \delta(\gamma - \gamma_k) \delta(t - t_k) \quad (\text{C.7})$$

we find the solution

$$S(x, T) = \sum_{k=0}^m q_k H(T - T(\tau_k)) \delta(x - x_k - T(\tau) + T(\tau_k)). \quad (\text{C.8})$$

With $x_k \geq 0$ and the solution (C.6) the integro-differential equation (C.4) reads

$$\frac{dT}{d\tau} = q_0 \frac{H(T - T(\tau_0))}{T - T(\tau_0) + x_0} + q_1 \frac{H(T - T(\tau_1))}{T - T(\tau_1) + x_1}. \quad (\text{C.9})$$

Since $dT/d\tau = \int_0^\infty \gamma n d\gamma \geq 0$ is an averaged energy density that vanishes only before the first injection and after all injected particles have cooled down, T is required to be strictly increasing in the time between. Hence, the image set $T = \{T(\tau_0) < T(\tau_1) \leq T(\tau)\}$ can be reduced to the subset $T = \{T(\tau_0) < T(\tau_1) \leq T(\tau) \mid \tau_0 < \tau_1 \leq \tau\}$ which is analogous to the equivalences $H(T - T(\tau_0)) \Leftrightarrow H(\tau - \tau_0)$ and $H(T - T(\tau_1)) \Leftrightarrow H(\tau - \tau_1)$, so that within the interval $\tau_0 < \tau_1 \leq \tau$ equation (C.9) yields

$$\frac{dT}{d\tau} = \frac{q_0}{T - T(\tau_0) + x_0} + \frac{q_1}{T - T(\tau_1) + x_1}. \quad (\text{C.10})$$

This differential equation can be converted into the simpler form

$$\frac{dT}{d\tau} = \frac{qT + q_0s_1 + q_1s_0}{T^2 + (s_0 + s_1)T + s_0s_1}, \quad (\text{C.11})$$

where $q \equiv q_0 + q_1$ and $s_k \equiv x_k - T(\tau_k)$. A transformation with the function $\xi = qT + q_0s_1 + q_1s_0$ and the constants $z_0 \equiv (s_0 - s_1)(q_0 - q_1)$ and $z_1 \equiv q_0q_1(s_0 - s_1)^2$ leads to the equation

$$\frac{d\xi}{d\tau} = \frac{q^3\xi}{\xi^2 + z_0\xi - z_1}, \quad (\text{C.12})$$

which can be easily integrated yielding

$$\int \frac{\xi^2 + z_0\xi - z_1}{\xi} d\xi = \frac{\xi^2}{2} + z_0\xi - z_1 \ln(\xi) = q^3\tau + \text{const.} \quad (\text{C.13})$$

This transcendental equation has to fulfil the relations $\xi \geq 0$ and $d\xi/d\tau \geq 0$, resulting in the inequality

$$\xi^2 + z_0\xi - z_1 > 0 \quad (\text{C.14})$$

with the solutions $\xi > q_1(s_0 - s_1)$ for $s_0 - s_1 > 0$ and $\xi > -q_0(s_0 - s_1)$ for $s_0 - s_1 < 0$. To obtain analytical solutions of equation (C.13), we analyse the two domains $\xi \ll 1$ and $\xi \gg 1$.

C.1 The case $\xi \gg 1$

For $\xi \gg 1$ equation (C.13) approximately reads

$$\frac{\xi^2}{2} + z_0\xi = q^3\tau + \text{const.}, \quad (\text{C.15})$$

which can be easily solved using the quadratic formula. The constant can be determined by applying the boundary condition $T(\tau_1)$ at the time of the second injection. So one obtains for the initial function T

$$T(\tau) = \hat{q}_0(T(\tau_0) - x_0) + \hat{q}_1(T(\tau_1) - x_1) + \sqrt{2q(\tau - \tau_1) + (\hat{q}_0[T(\tau_1) - T(\tau_0) + x_0] + \hat{q}_1 x_1)^2}, \quad (\text{C.16})$$

where $\hat{q}_k \equiv q_k/q$. To calculate $T(\tau_0)$ and $T(\tau_1)$ the intervals $\tau < \tau_0 < \tau_1$ and $\tau_0 \leq \tau < \tau_1$ have to be examined first.

Throughout the whole time interval $\tau < \tau_0 < \tau_1$ differential equation (C.9) leads to the solution $T(\tau) = 0$. To assure the continuity of T at the transition of the intervals it is inevitable to demand that $T(\tau_0) = 0$. With this condition equation (C.9) reads for $\tau_0 \leq \tau < \tau_1$

$$\frac{dT}{d\tau} = \frac{q_0}{T + x_0} \quad (\text{C.17})$$

leading to

$$x_0 T + \frac{T^2}{2} = q_0 \tau + \text{const.}, \quad (\text{C.18})$$

where $\text{const.} = -q_0 \tau_0$. This equation is solved by

$$T(\tau) = -x_0 + \sqrt{2q_0(\tau - \tau_0) + x_0^2}. \quad (\text{C.19})$$

Again it is essential to require in order to guarantee the continuity of T the constant $T(\tau_1)$ to be

$$T(\tau_1) = -x_0 + \sqrt{2q_0(\tau_1 - \tau_0) + x_0^2}. \quad (\text{C.20})$$

The second solution of (C.16) and (C.19) can be omitted because we demanded $T(\tau)$ to be strictly increasing over the complete time interval.

In terms of τ the solution (C.6) reads for the different time domains

$$S(x, T | \tau_0 \leq \tau < \tau_1) = q_0 H(x - x_0) \delta\left(x - \sqrt{2q_0(\tau - \tau_0) + x_0^2}\right) \quad (\text{C.21})$$

and

$$\begin{aligned}
 S(x, T | \tau_0 < \tau_1 \leq \tau) &= q_0 H(x - x_0) \\
 &\cdot \delta \left(x - \sqrt{2q(\tau - \tau_1) + \left(\hat{q}_1 x_1 + \hat{q}_0 \sqrt{2q_0(\tau_1 - \tau_0) + x_0^2} \right)^2} \right. \\
 &\left. + \hat{q}_1 \left(x_1 - \sqrt{2q_0(\tau_1 - \tau_0) + x_0^2} \right) \right) + q_1 H(x - x_1) \\
 &\cdot \delta \left(x - \sqrt{2q(\tau - \tau_1) + \left(\hat{q}_1 x_1 + \hat{q}_0 \sqrt{2q_0(\tau_1 - \tau_0) + x_0^2} \right)^2} \right. \\
 &\left. + \hat{q}_0 \left(\sqrt{2q_0(\tau_1 - \tau_0) + x_0^2} - x_1 \right) \right).
 \end{aligned} \tag{C.22}$$

With these the nonlinear solution for the electron density distribution $n(\gamma, t)$ can be calculated to

$$n(\gamma, t | t_0 \leq t < t_1) = q_0 H(\gamma_0 - \gamma) \delta(\gamma - \gamma_{NL}) \tag{C.23}$$

$$n(\gamma, t | t_0 < t_1 \leq t) = q_0 H(\gamma_0 - \gamma) \delta(\gamma - \gamma_{NL}^{(0)}) + q_1 H(\gamma_1 - \gamma) \delta(\gamma - \gamma_{NL}^{(1)}), \tag{C.24}$$

where

$$\gamma_{NL} = \frac{\gamma_0}{\sqrt{1 + 2q_0 A_0 \gamma_0^2 (t - t_0)}} \tag{C.25}$$

is the characteristic nonlinear Lorentz factor for the single-injection scenario and

$$\begin{aligned}
 \gamma_{NL}^{(k)} &= \gamma_0 \gamma_1 \left(\sqrt{2q A_0 \gamma_0^2 \gamma_1^2 (t - t_1) + \left(\hat{q}_1 \gamma_0 + \hat{q}_0 \gamma_1 \sqrt{2q_0 A_0 \gamma_0^2 (t_1 - t_0) + 1} \right)^2} \right. \\
 &\left. + (-1)^k \hat{q}_{|k-1|} \left(\gamma_1 \sqrt{2q_0 A_0 \gamma_0^2 (t_1 - t_0) + 1} - \gamma_0 \right) \right)^{-1}
 \end{aligned} \tag{C.26}$$

are the characteristic nonlinear Lorentz factors for the double-injection scenario with $k = 0, 1$.

C.2 The case $\xi \ll 1$

Considering the boundary inequality (C.14) coupled to the special case $\xi \ll 1$ we obtain the relation

$$q_1(s_0 - s_1) < \xi \ll 1 \quad \text{for} \quad s_0 > s_1 \quad \Rightarrow \quad q_1\left(\sqrt{2q_0(\tau_1 - \tau_0) + x_0^2} - x_1\right) \ll 1$$

and

$$-q_0(s_0 - s_1) < \xi \ll 1 \quad \text{for} \quad s_0 < s_1 \quad \Rightarrow \quad q_0\left(x_1 - \sqrt{2q_0(\tau_1 - \tau_0) + x_0^2}\right) \ll 1.$$

These particular relations hold only for small injection strengths q_k and for small injection sequences $\tau_1 - \tau_0$ assuming nearly identical injection energies γ_k . Here, both cases can be omitted because on the one hand the injection of relativistic particles of the ambient interstellar and intergalactic mediums into the plasmoid is of intense strength (order of magnitude $\sim 10^5$) due to the plasmoids size in correlation with the outer particle density and on the other hand the plasmoid collects relativistic particles sweeping through the interstellar and intergalactic mediums via a pick-up process, which is assumed here to be a discrete collection process, so that it is essential that the system consisting of the plasmoid and the interstellar and intergalactic mediums needs some time after each injection to adjust and collect enough particles for another injection.

D Optically thin synchrotron radiation intensities

The structure of the electron spectrum is given in both the linear and the nonlinear cooling cases by $n(\gamma, t) = q_0 H(\gamma_0 - \gamma) \delta(\gamma - \gamma^{(0)}(t)) + q_1 H(\gamma_1 - \gamma) \delta(\gamma - \gamma^{(1)}(t))$. Thus the synchrotron intensity (2.15) for the domain $t_0 < t_1 \leq t$ reads

$$I(\nu, t) = \frac{RP_0\nu}{4\pi} \left[q_0 \gamma^{(0)-2} CS\left(\frac{\nu}{\nu^{(0)}}\right) + q_1 \gamma^{(1)-2} CS\left(\frac{\nu}{\nu^{(1)}}\right) \right]. \quad (\text{D.1})$$

The linear cooling case yields

$$I_L(\nu, t) \simeq \frac{3RP_0\nu_0}{8\pi} \left(q_0 \left[0.869 \left(\frac{\nu_L^{(0)}}{\nu} \right)^{1/3} + \exp\left(\frac{\nu}{\nu_L^{(0)}}\right) \right]^{-1} + q_1 \left[0.869 \left(\frac{\nu_L^{(1)}}{\nu} \right)^{1/3} + \exp\left(\frac{\nu}{\nu_L^{(1)}}\right) \right]^{-1} \right) \quad (\text{D.2})$$

with the characteristic frequencies

$$\nu_L^{(k)} = \frac{3}{2} \nu_0 \gamma_L^{(k)2} = \frac{3\nu_0 \gamma_k^2}{2(1 + D_0 \gamma_k(t - t_k))}. \quad (\text{D.3})$$

In the nonlinear cooling case, however, the electron gyrofrequency is a function of time due to the time-dependence of the magnetic field

$$\nu_0(t) = \frac{eB(t)}{2\pi m_e c} = c \sqrt{2e_B r_0 \pi^{-1} \int_0^\infty \gamma n_{NL}(\gamma, t) d\gamma} = c \sqrt{2e_B r_0 \pi^{-1} (q_0 \gamma_{NL}^{(0)} + q_1 \gamma_{NL}^{(1)})}. \quad (\text{D.4})$$

The constant $r_0 = 2.82 \cdot 10^{-13}$ cm denotes the classical electron radius. Using the non-linear characteristic frequencies

$$\nu_{NL}^{(k)} = \frac{3}{2} \nu_0(t) \gamma_{NL}^{(k)2} = \frac{3}{2} c \sqrt{2e_B r_0 \pi^{-1} (q_0 \gamma_{NL}^{(0)} + q_1 \gamma_{NL}^{(1)})} \gamma_{NL}^{(k)2} \quad (\text{D.5})$$

the nonlinear optically thin synchrotron intensity can be obtained

$$I_{NL}(\nu, t) \simeq \frac{3RP_0c}{8\pi} \sqrt{2e_B r_0 \pi^{-1} (q_0 \gamma_{NL}^{(0)} + q_1 \gamma_{NL}^{(1)})} \cdot \left[q_0 \left(0.869 \left(\frac{\nu_{NL}^{(0)}}{\nu} \right)^{1/3} + \exp \left(\frac{\nu}{\nu_{NL}^{(0)}} \right) \right)^{-1} + q_1 \left(0.869 \left(\frac{\nu_{NL}^{(1)}}{\nu} \right)^{1/3} + \exp \left(\frac{\nu}{\nu_{NL}^{(1)}} \right) \right)^{-1} \right]. \quad (\text{D.6})$$

The detailed calculations for the domain $t_0 \leq t < t_1$ can be found in the appendices of Schlickeiser and Lerche (2007).

E Synchrotron optical depth and photon spectra

E.1 Optical depth

The synchrotron emission of ultra-relativistic electrons is optically thin for frequencies and times satisfying the condition $D(\omega, \tau) \leq 1$ and optically thick for $D(\omega, \tau) > 1$. The transition occurs at the frequency $\omega_t(\tau)$ defined by $D(\omega, \tau) = 1$. For $\tau - \tau_0 \ll 1$ (and its analytical continuation) the optical depth (3.9) reduces to

$$D(\omega, \tau - \tau_0 \leq 1) \simeq \left(\frac{\omega_1}{\omega}\right)^{5/3} (1 + \tau - \tau_0)^{2/3} \quad (\text{E.1})$$

as long as $\tau - \tau_0 \leq \omega^{-4/5}$. In this range the transition frequency reads

$$\omega_t(\tau - \tau_0 \leq \omega^{-4/5}) \simeq \omega_1(1 + \tau - \tau_0)^{2/5}. \quad (\text{E.2})$$

In the domain $\tau - \tau_0 \gg 1$ (and its analytical continuation) the optical depth simplifies to

$$D(\omega, \tau - \tau_0 > 1) \simeq \left(\frac{\omega_1}{\omega}\right)^{5/3} (\tau - \tau_0)^{2/3} \left(1 + \frac{3}{2}\omega(\tau - \tau_0)^{5/4}\right) \exp\left(-\omega(\tau - \tau_0)^{5/4}\right). \quad (\text{E.3})$$

Substituting $z = \omega(\tau - \tau_0)^{5/4}$ and expanding asymptotically for $z > 1$ as well as for $z \leq 1$ we find

$$D(z) = \omega_1^{5/3} \omega^{-11/5} z^{8/15} \left(1 + \frac{3}{2}z\right) e^{-z} \simeq \omega_1^{5/3} \omega^{-11/5} \begin{cases} z^{8/15} & , z \leq 1 \\ \frac{3}{2} z^{23/15} e^{-z} & , z > 1 \end{cases} \quad (\text{E.4})$$

with the proper transition frequency

$$\omega_t(\tau) \simeq \begin{cases} \omega_1(\tau - \tau_0)^{2/5} & , \tau - \tau_0 \leq \omega_1^{-20/33} \\ (\tau - \tau_0)^{-5/4} \ln \left(\frac{3}{2} \omega_1^{5/3} (\tau - \tau_0)^{11/4} \right) & , \tau - \tau_0 > \omega_1^{-20/33}. \end{cases} \quad (\text{E.5})$$

In Figure E.1, we present the time-dependence of the transition frequency. For small times $\tau - \tau_0 \leq 1$ the transition frequency is constant at the value ω_1 . After this it increases linearly to its maximum $\omega_1^{25/33}$ at $\tau - \tau_0 = \omega_1^{-20/33}$ followed by a decrease proportional to $\tau^{-5/4}$ at times $\tau - \tau_0 > \omega_1^{-20/33}$.

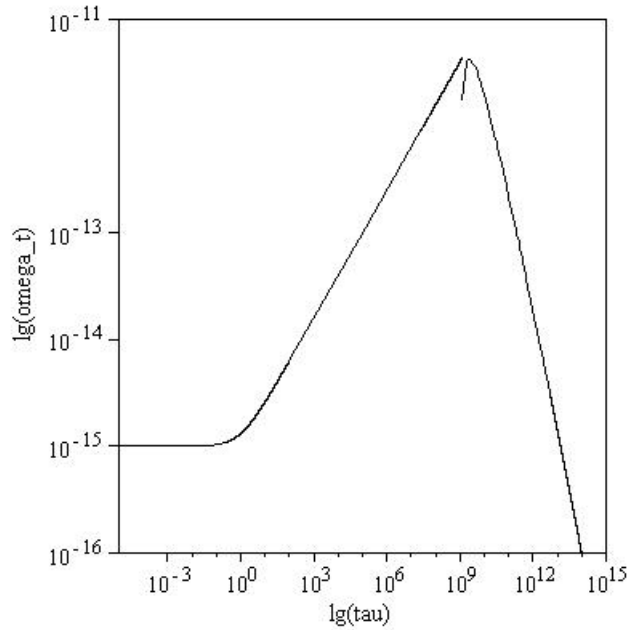


Figure E.1: Normalised synchrotron transition frequency ω_t as a function of the time τ in the nonlinear cooling case plotted for $\omega_1 = 10^{-15}$. The instantaneous injection of monoenergetic ultra-relativistic electrons occurred at $\tau_0 = 0$.

E.2 Synchrotron spectra

According to (3.5) the synchrotron intensity in the optically thick frequency domain $\omega \leq \omega_t$ is given by

$$I(\omega \leq \omega_t, \tau) \simeq \frac{j(\omega, \tau)R}{D(\omega, \tau)} = I_0 \omega_1^{-5/3} \frac{\omega^2}{(1 + \tau - \tau_0)^{1/2} \left(1 + \frac{3}{2}\omega(1 + \tau - \tau_0)^{5/4}\right)}, \quad (\text{E.6})$$

where $I_0 \equiv a_0 P_0 q_0 R \nu_0 / (4\pi)$. In the optically thin frequency interval $\omega > \omega_t$ we obtain

$$I(\omega > \omega_t, \tau) \simeq j(\omega, \tau)R = I_0 \omega^{1/3} (1 + \tau - \tau_0)^{1/6} \exp(-\omega(1 + \tau - \tau_0)^{5/4}). \quad (\text{E.7})$$

In Figure E.2, we show the intensity distribution as a function of the frequency ω at various times $\tau = 0, 10^4, 10^9$ and 10^{11} . Consequently the transition intensity reads

$$I_{trans}(\tau) = I(\omega_t, \tau) = I_0 \omega_1^{-5/3} \frac{\omega_t^2}{(1 + \tau - \tau_0)^{1/2} \left[1 + \frac{3}{2}\omega_t(1 + \tau - \tau_0)^{5/4}\right]}. \quad (\text{E.8})$$

Applying the transition frequencies (E.2) and (E.5) we obtain for the transition intensity at normalised times $\tau - \tau_0 \leq \omega_1^{-20/33}$

$$I_{trans}(\tau - \tau_0 \leq \omega_1^{-20/33}) \simeq I_0 \frac{\omega_1^{1/3} (1 + \tau - \tau_0)^{3/10}}{1 + \frac{3}{2}\omega_1 (1 + \tau - \tau_0)^{33/20}}, \quad (\text{E.9})$$

whereas at times $\tau - \tau_0 > \omega_1^{-20/33}$ the result is

$$I_{trans}(\tau - \tau_0 > \omega_1^{-20/33}) \simeq \frac{2I_0}{3\omega_1^{5/3}} \frac{\ln\left(\frac{3}{2}\omega_1^{5/3}(\tau - \tau_0)^{11/4}\right)}{(\tau - \tau_0)^3}. \quad (\text{E.10})$$

At small times $\tau - \tau_0 \leq 1$ the transition intensity turns out to be

$$I_{trans}(\tau - \tau_0 \leq 1) \simeq I_0 \omega_1^{1/3}. \quad (\text{E.11})$$

The time-dependence of the transition intensity is presented in Figure E.3.

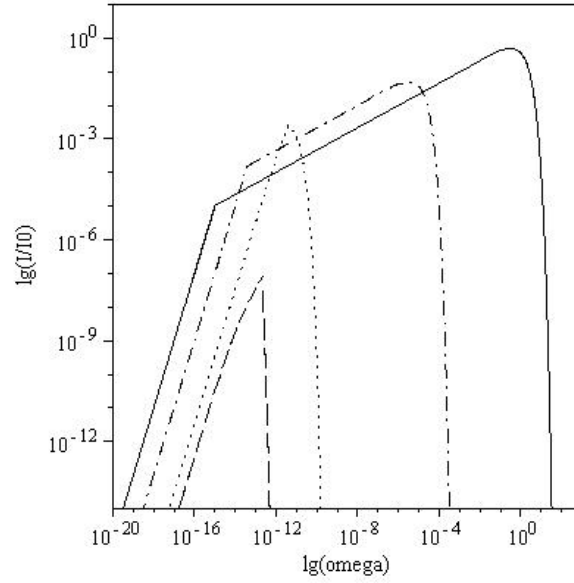


Figure E.2: Synchrotron intensity distribution as a function of the frequency ω at different times $\tau = 0$ (solid curve), $\tau = 10^4$ (dash-dotted curve), $\tau = 10^9$ (dotted curve) and $\tau = 10^{11}$ (dashed curve). The injection occurred at $\tau_0 = 0$ with the parameter $\omega_1 = 10^{-15}$.

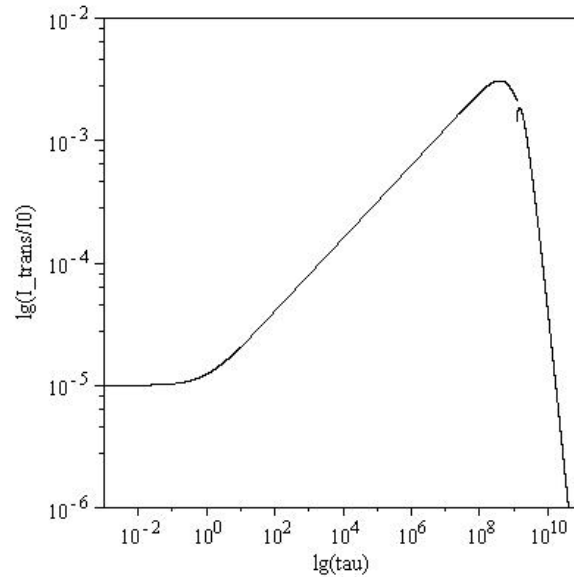


Figure E.3: Synchrotron transition intensity I_{trans}/I_0 as a function of the time τ plotted for $\omega_1 = 10^{-15}$ at the injection time $\tau_0 = 0$.

Bibliography

- Abel, N.H., Journal für die reine und angewandte Mathematik **1**, 65 (1826)
- Abramowitz, M., Stegun, I. S., "Handbook of Mathematical Functions", Dover Publications, New York (1972)
- Aharonian, F., et al. (H.E.S.S. Collaboration), Science **314**, 1424 (2006)
- Aharonian, F., et al. (H.E.S.S. Collaboration), ApJ **664**, L71 (2007)
- Akaike, H., IEEE Transactions on Automatic control **19**, 716 (1974)
- Antonucci, R., Annu. Rev. Astron. Astrophys. **31**, 473 (1993)
- Arbeiter, C., Pohl, M., Schlickeiser, R., A&A **386**, 415 (2002)
- Arbeiter, C., Dissertation (2005)
- Arbeiter, C., Pohl, M., Schlickeiser, R., ApJ **627**, 62 (2005)
- Blazejowski, M., et al., ApJ **545**, 107 (2000)
- Blumenthal, G.R., Gould, R.J., Rev. Mod. Phys. **42**, 237 (1970)
- Böttcher, M., Chiang, J., ApJ **581**, 127 (2002)
- Böttcher, M., Reimer, A., ApJ **609**, 576 (2004)
- Böttcher, M., Astrophys. & Space Sci. **309**, 95 (2007)
- Chiaberge, M., Ghisellini, G., MNRAS **306**, 551 (1999)
- Crusius, A., Schlickeiser, R., A&A **164**, L16 (1986)
- Crusius, A., Schlickeiser, R., A&A **196**, 327 (1988)

- Dermer, C.D., Schlickeiser, R., *Science* **257**, 1642 (1992)
- Dermer, C.D., Schlickeiser, R., Mastichiadis, A., *A&A* **256**, L27 (1992)
- Dermer, C.D., Schlickeiser, R., *ApJ* **416**, 458 (1993)
- Dermer, C.D., Sturmer, S.J., Schlickeiser, R., *ApJ Suppl.* **109**, 103 (1997)
- Dermer, C.D., Schlickeiser, R., *ApJ* **575**, 667 (2002)
- Frederiksen, et al., *ApJ* **608**, L13 (2004)
- Gerbig, D., Schlickeiser, R., *ApJ* **664**, 750 (2000)
- Ghisellini, G., et al., *ApJ* **407**, 65 (1993)
- Jaroschek, C., Lesch, H., Treumann, R., *ApJ* **618**, 822 (2005)
- Jauch, J.M., Rohrlich, F., "The Theory of Photons and Electrons", Springer (1976)
- Jones, F.C., *Phys. Rev.* **167**, 1159 (1968)
- Kapetanakos, C.A., *Applied Physics Letters* **25**, 484 (1974)
- Kardashev, N.S., *Soviet Astronomy* **6**, 317 (1962)
- Lee, R., Lampe, M., *Phys. Rev. Lett.* **31**, 1390 (1973)
- Maraschi, L., Ghisellini, G., Celotti, A., *ApJ* **397**, L5 (1992)
- Mastichiadis, A., Kirk, J. G., *A&A* **320**, 19 (1997)
- Mastichiadis, A., Kirk, J. G., *Publ. Astron. Soc. Aust.* **19**, 1 (2002)
- Medvedev, M.V., et al., *ApJ* **666**, 339 (2007)
- Mutel, R.L., et al., *ApJ* **352**, 81 (1990)
- Ng, J.S.T., Noble, R.J., *Phys. Rev. Lett.* **96**, 115006 (2006)
- Nishikawa, K.I., et al., *ApJ* **595**, 555 (2003)
- Pohl, M., Schlickeiser, R., *A&A* **354**, 395 (2000)
- Reimer, A., Protheroe, R.J., Donea, A.C., *New Astronomy Review* **48**, 411 (2004)

- Reynolds, S.P., ApJ **256**, 38 (1982)
- Sakai, J.I., Schlickeiser, R., Sukla, P.K., Phys. Lett. A **330**, 384 (2004)
- Schlickeiser, R., "Cosmic Ray Astrophysics", Springer-Verlag, Berlin (2002)
- Schlickeiser, R., A&A **410**, 397 (2003)
- Schlickeiser, R., Lerche, I., A&A **476**, 1 (2007)
- Schlickeiser, R., Lerche, I., A&A **485**, 315 (2008)
- Schlickeiser, R., Röken, C., A&A **477**, 701 (2008)
- Sikora, M., Begelman, M.C., Rees, M.J., ApJ **421**, 153 (1994)
- Silva, L. O., et al., ApJ **596**, L121 (2003)
- Sokolov, A., Marscher, A.P., McHardy, I.M., ApJ **613**, 725 (2004)
- Stockem, A., Lerche, I., Schlickeiser, R., ApJ **659**, 419 (2007)
- Tatarakis, M., et al., Phys. Rev. Lett. **90**, 175001 (2003)
- Weekes, T.C., Phys. Scr. **T85**, 195 (2000)
- Workman, J.C., et al., MNRAS **386**, 199 (2008)
- Xie, G.Z., et al., A&A **278**, 6 (1993)

Danksagung

An dieser Stelle möchte ich mich bei all denen bedanken, die mich dabei unterstützt haben, diese Doktorarbeit zu erstellen. Mein besonderer Dank gilt

- Prof. Dr. Reinhard Schlickeiser für die Anregung zu dieser Arbeit, die dazugehörige Betreuung und Förderung, sowie für die zahlreichen Hinweise und Diskussionen
- PD Dr. Horst Fichtner für die Bereitschaft zur Übernahme des Koreferates und für das hilfreiche Korrekturlesen der Arbeit
- Dr. Andreas Kopp für die nützlichen Hinweise und Korrekturen
- meiner Freundin Katharina für die Unterstützung, das Korrekturlesen und dafür, dass sie immer für mich da war
- meinen Eltern für den familiären Rückhalt und die ständige Unterstützung

Lebenslauf

Kontakt

Christian Röken

Institut für Theoretische Physik

Lehrstuhl IV: Weltraum - und Astrophysik

Ruhr-Universität Bochum

44780 Bochum

Deutschland

Telefon: +49 (0)234 3223771

E-mail: cr@tp4.rub.de

Persönliches

Geburtsdatum: 26.04.1983

Geburtsort: Gelsenkirchen

Staatsangehörigkeit: deutsch

Bildungsweg

Abitur, Mai 2002

Carl-Friedrich Gauss Gymnasium

Gelsenkirchen

Diplom, Theoretische Physik, Mathematische Physik, März 2007

Ruhr-Universität Bochum

Thema: Emission von Spin-1/2-Fermionen durch rotierende Schwarze
Löcher

Betreuer: Prof. Dr. Ian Lerche, Prof. Dr. Reinhard Schlickeiser

Promotion, Theoretische Physik, seit April 2007

Ruhr-Universität Bochum

Thema: Nonlinear electron synchrotron cooling and synchrotron
self-Compton flaring of TeV blazars

Betreuer: Prof. Dr. Reinhard Schlickeiser